

Exploiting Unlabeled Data with Multiple Expert Teachers for Open Vocabulary Aerial Object Detection and Its Orientation Adaptation

Yan Li, Weiwei Guo, *Member, IEEE*, Xue Yang, Ning Liao, Shaofeng Zhang
Yi Yu, Wenxian Yu, *Senior Member, IEEE*, Junchi Yan, *Senior Member, IEEE*

Abstract—In recent years, aerial object detection has been increasingly pivotal in various earth observation applications. However, current algorithms are limited to detecting a set of pre-defined object categories, demanding sufficient annotated training samples, and fail to detect novel object categories. In this paper, we put forth a novel formulation of the aerial object detection problem, namely open-vocabulary aerial object detection (OVAD), which can detect objects beyond training categories without costly collecting new labeled data. We propose CastDet, a CLIP-activated student-teacher detection framework that serves as the first OVAD detector specifically designed for the challenging aerial scenario, where objects often exhibit weak appearance features and arbitrary orientations. Our framework integrates a robust localization teacher along with several box selection strategies to generate high-quality proposals for novel objects. Additionally, the RemoteCLIP model is adopted as an omniscient teacher, which provides rich knowledge to enhance classification capabilities for novel categories. A dynamic label queue is devised to maintain high-quality pseudo-labels during training. By doing so, the proposed CastDet boosts not only novel object proposals but also classification. Furthermore, we extend our approach from horizontal OVAD to oriented OVAD with tailored algorithm designs to effectively manage bounding box representation and pseudo-label generation. Extensive experiments for both tasks on multiple existing aerial object detection datasets demonstrate the effectiveness of our approach. The code is available at <https://github.com/lizzy8587/CastDet>.

Index Terms—Open-vocabulary aerial detection, Oriented object detection, Semi-supervised learning, Multi-modal.

I. INTRODUCTION

OBJECT detection in aerial images aims at localizing and categorizing objects on the earth’s surface, which is fundamental to a wide range of remote sensing applications, such as urban planning, environmental surveillance, and disaster response [1]–[3]. Despite significant advancements in aerial object detectors powered by deep learning [4]–[9], they are still weak at detecting objects beyond the training categories.

To expand the object detectors to novel categories, a naive idea is to collect and annotate large-scale aerial images with

Yan Li, Xue Yang, Ning Liao, Shaofeng Zhang, Wenxian Yu and Junchi Yan are with Shanghai Jiao Tong University, Shanghai, 200240, China (e-mail: daodao123@sjtu.edu.cn, yangxue-2019-sjtu@sjtu.edu.cn, liaoning@sjtu.edu.cn, sherryone@sjtu.edu.cn, wxyu@sjtu.edu.cn, yanjunchi@sjtu.edu.cn).

Weiwei Guo is the corresponding author with Tongji University, Shanghai, 200092, China (email: weiweiguo@tongji.edu.cn), and Wenxian Yu is the Co-corresponding author.

Yi Yu is with School of Automation, Southeast University, Nanjing, 210096, China (e-mail: yuyi@seu.edu.cn).

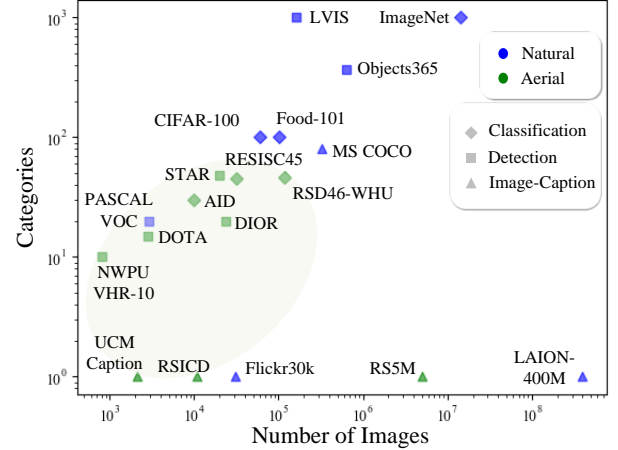


Fig. 1. Comparisons of the amount of categories and images of 19 common aerial and natural datasets. **Challenge 1: Aerial datasets are much smaller in size and category vocabularies compared with natural image datasets.**

rich object categories. However, obtaining accurate yet sufficient annotations is time- and labor-expensive, even requiring human experts involvement. As a result, despite extensive efforts paid in the collection of existing aerial object detection datasets [10]–[15], they are still much smaller and less diverse than natural image datasets [16]–[18], as depicted in Fig. 1. It hinders the detector scaling up in open-world scenarios. Therefore, this paper advocates more flexible object detectors capable of detecting novel object categories unseen during training, referred to as open vocabulary object detection (OVD). This allows us to characterize new objects that emerged in the earth observation data without extra annotations in open scenarios.

Drawing inspiration from the recent success of OVD in natural images [19]–[21], we intend to explore ways in the challenging task, namely open vocabulary aerial object detection (OVAD), where objects often vary widely in scale, orientation, and exhibit weak feature appearance [22]. Unlike natural images, which often feature clear contours and textures, allowing class-agnostic region proposal networks (RPNs) to effectively generalize to novel categories [23], [24]; aerial images captured from overhead perspectives usually display weak surface features, where objects may blend into the background. This complicates object detection, for instance, AIRPORT may be confused with HIGHWAY, and thus be wrongly classified as background, as illustrated in Fig. 2(b). Consequently, the

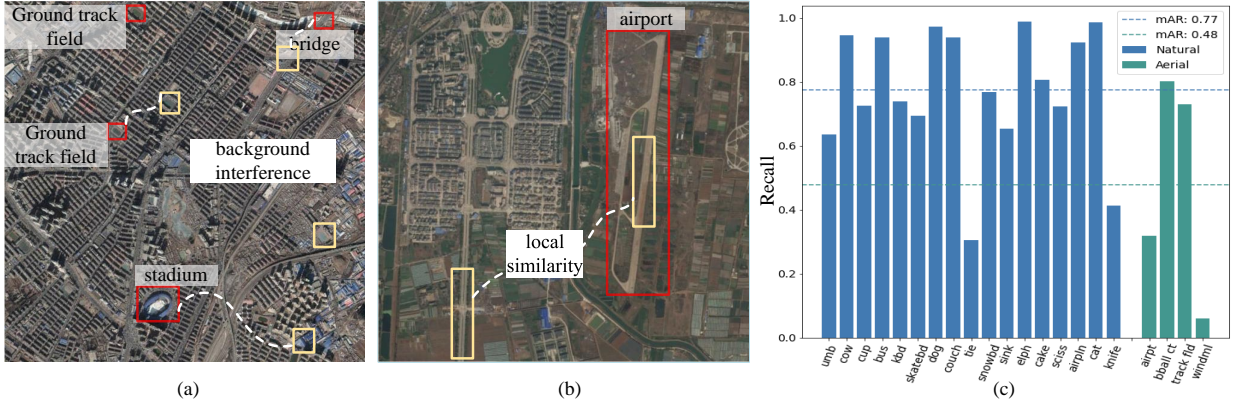


Fig. 2. **Challenge 2: The recall of novel objects in aerial images is much lower than that in natural images due to the highly complex backgrounds.** (a)(b) Aerial images from DIOR [11]. Objects in aerial images exhibit background interference. (c) Class-agnostic RPN recall statistics of novel categories in the natural dataset COCO [16] and the aerial dataset VisDroneZSD [25] (i.e., 77% v.s. 48%).

recall of novel categories in aerial images is significantly lower than that in natural images, as shown in Fig. 2(c). In addition, objects in aerial images exhibit great orientation diversity. Using horizontal bounding boxes for these rotated objects could bring in substantial background clutter, leading to inaccurate localization. However, current open-vocabulary detectors primarily support horizontal detection, which limits their effectiveness in aerial images. These factors, on the one hand, pose challenges to directly apply current OVD methods for natural images to aerial images; and, on the other hand, spur us to develop extensible object detectors for aerial images, covering more object categories without extra annotation.

To address these challenges, we propose a simple yet effective open-vocabulary aerial detection framework, namely **CastDet**, a **CLIP-activated student-teacher detector**. It comprises three key models: a student model and two teacher models for localization and classification, respectively. The student model is responsible for training both horizontal and oriented open-vocabulary detectors. The former adopts methods such as Faster R-CNN [26], and the later exploits the Oriented R-CNN [27]. The localization teacher model focuses on discovering and localizing potential objects, while the other teacher model provides classification guidance for novel categories. We jointly train the student model and teacher models in a self-learning manner, where the student is optimized with pseudo-labels generated by the teachers, and the localization teacher is updated from the continually learned student model. As exemplified by the literature [28], the slowly progressing localization teacher model acts as an ensemble of the previous student models, exhibiting superior capabilities that enable it to generate more reliable proposals. These proposals are then filtered based on their confidence scores, such as scale jittering variance, before being presented to the external teacher.

While the student-teacher learning paradigm is powerful for enhancing the capabilities of the student model under the guidance of the teacher model [28]–[32], they operate in the closed-set setting. This leads to poor performance in discovering and recognizing novel object categories that are not encountered in the training data. To overcome this limitation, RemoterCLIP [33] that has been pre-trained on

massive remote sensing image-text pairs and equips with strong zero-shot classification capabilities is exploited as an external teacher model. Thus, the learning process could benefit from the extra knowledge dedicated to interpreting aerial images brought by the RemoteCLIP. In addition to involving the RemoteCLIP, maintaining high-quality pseudo-labels is necessary. To this end, after predicting the category labels for the pseudo proposals, a dynamic label queue is proposed to store and iteratively update the pseudo-labels.

Unlike previous CLIP-based methods [23], [34], [35] that directly transfer knowledge from CLIP for open-vocabulary recognition, our CLIP-activated student-teacher self-learning framework incorporates high-confidence knowledge from RemoteCLIP as an incentive to guide both the student and localization teacher. This self-learning mechanism facilitates a “flywheel effect” wherein the external teacher transfers knowledge to strengthen the localization teacher to identify potential regions of novel objects, thereby enhancing pseudo box quality. In turn, the refined pseudo boxes enable the external teacher to produce more precise pseudo-labels. Through our student-teacher self-learning process, the detection model can be progressively updated to localize and recognize continuously expanded object category vocabularies.

The preliminary content of this paper has partially appeared in the conference version, with the detector named CastDet [36] (ECCV 2024). The overall contributions of this extended journal version are as follows¹:

- 1) Our work pioneers the open vocabulary aerial object detection (OVAD) to conquer fundamental challenges

¹This journal version extends the previous conference version (ECCV 2024) [36], particularly in the following aspects: **1)** We rewrite the full paper with comprehensive discussions and more details; **2)** The proposed CastDet framework is now extended to support open-vocabulary oriented detection, addressing the specific challenges of detecting objects with arbitrary orientations in aerial scenes; **3)** We introduce two new oriented box selection strategies: box scale jittering variance and angle jittering variance, which take both the scale and orientation of objects into account to filter robust pseudo boxes; **4)** We integrate multiple open-vocabulary oriented detection algorithms into a unified code repository, including Oriented CastDet, Oriented ViLD, Oriented GLIP and Oriented GroundingDINO; **5)** We conduct more ablation experiments to demonstrate the effectiveness of the proposed techniques; **6)** We build a more comprehensive benchmark for the open-vocabulary aerial detection task, including both horizontal object detection and oriented object detection.

in interpreting earth observation images: the relatively small scale of annotated data in terms of both the number of training samples and the object categories; and the unique characteristics of aerial images, such as arbitrary orientations and weak feature appearances.

- 2) We introduce the CastDet, a flexible open-vocabulary detection framework incorporating the student-(multi)teacher self-learning paradigm. The proposed framework enables the detection model to progressively expand its object vocabulary and achieve accurate localization of novel objects using horizontal or oriented boxes without extra annotation efforts.
- 3) We propose a series of box selection strategies to preserve high-quality pseudo-labels via filtering, including RPN Score, box jittering variance (BJV) and regression jittering variance (RJV) for horizontal boxes; scale jittering variance (SJV) and angle jittering variance (AJV) for oriented boxes.
- 4) We devise a dynamic label queue for storing and incrementally updating high-quality pseudo-labels generated by the teachers. By this way, richer and more accurate labels could be dynamically maintained.
- 5) We implement multiple open-vocabulary oriented object detection methods, including Oriented ViLD, Oriented GLIP and Oriented GroundingDINO. This marks the first effort to open-vocabulary oriented detection.
- 6) We utilize several public aerial image datasets to establish the open-vocabulary aerial detection benchmark and conduct extensive experiments to validate our methods, achieving significant performance improvement.

II. RELATED WORK

A. Fully-supervised Object Detection

Object detection aims to predict the bounding box coordinates and corresponding category labels for objects of interest within an image. Generally, existing object detection methods can be divided into two-stage and one-stage methods. Two-stage methods [26], [37]–[40] such as Faster R-CNN [26] initially employ a region proposal network to generate potential target regions, then classify and refine these proposals. One-stage methods model the object localization and categorization as an end-to-end problem, which is to be resolved through a single network. Classical methods include anchor-based ones, such as YOLO [41], SSD [42], RetinaNet, [43], and anchor-free methods, e.g., CornerNet [44], FCOS [45], CenterNet [46].

Inspired by the advanced progress of object detection methods [22], [26], [41], [43], [47] dedicated to natural images, efforts have been paid to adapt these methods to aerial images. Specifically, several challenges remains to be tackled in aerial images, including object orientation [5]–[7], [27], [48], scale variation [49], [50], and dense objects [8], [9], [51], [52]. Early works [4], [53]–[55] mainly focus on horizontal detection using classical deep learning methods to detect aerial objects with horizontal bounding boxes. However, horizontal bounding box could cause inaccurate location of aerial objects with arbitrary orientations. Therefore, methods

that could represent objects by oriented bounding boxes [51], [56] have attracted widespread attention. One focus of research is on optimizing the representation of oriented objects, which can be achieved by converting the angle regression task into an angle classification task [57], [58] or by modeling oriented objects using a Gaussian distribution [59]–[61]. In parallel, other studies emphasize learning robust alignment feature for oriented objects, exemplified by approaches such as SCRDet [8], R³Det [6], S²A-Net [62], and ReDet [48].

B. Semi-supervised Object Detection

Semi-supervised learning (SSL) incorporates external unlabeled data to improve performance through various techniques, including data augmentation [63]–[65], pseudo-labeling [66]–[68], and consistency training [69]–[72]. CSD [29] trains the detector to match the predictions between the original and horizontal flipped images. STAC [30] generates high confidence offline pseudo-labels from unlabeled images, and updates the detector through consistency training with strong augmentations. Instant-Teaching [31] updates pseudo-labels during the model training thus improving the quality of pseudo annotations. Furthermore, several works incorporate an Exponential Moving Average (EMA) strategy inspired by the Mean Teacher [70] to continuously update the teacher model [28], [32], [73], [74]. Among these, Unbiased Teacher [28] further addresses pseudo-label bias through focal loss; Soft-Teacher [32] employs soft labels weighted by confidence scores, and a box jittering strategy to select reliable pseudo boxes for training the box regression branch.

Recent studies have explored semi-supervised oriented object detection [75]–[79], which presents additional challenges due to the arbitrary orientations of objects. SOOD [75], [80] proposes rotation-aware adaptive weighting loss and global consistency loss for semi-supervised oriented object detection. S²O-Det [79] introduces coarse-to-fine sample mining strategy for selecting discriminative pseudo-labels. Focal Teacher [77] employs a global focal learning method to generate high-quality pseudo-labels without relying on artificial priors. Despite these advances, existing methods still face certain limitations. Current aerial object detectors operate under a closed-set assumption, where all categories of interest are annotated before training. Detectors trained in such a closed-set manner struggle to identify novel categories, limiting their adaptability to open world.

C. Open-vocabulary Object Detection

Open-vocabulary object detection (OVD) aims to detect objects beyond a close-set vocabularies. OVR-CNN [81] pioneered this approach by combining bounding box annotations for a subset of categories with a corpus of image-caption pairs to extend the vocabulary of detectable objects. Leveraging the zero-shot capabilities of pre-trained Vision-Language Models (VLMs), such as CLIP [82], recent OVD methods transfer knowledge from pre-trained VLMs through prompt learning [83]–[85] or region-level fine-tuning [24], [34], [35], [86] to achieve flexible and versatile detection of extensible object categories. For instance, ViLD [34] transfers knowledge

from a pre-trained VLM to enrich a two-stage detector through both vision and language knowledge distillation. RegionCLIP [35] aligns visual representations at the region level with text descriptions. Detic [24] enhances the vocabularies by incorporating image classification data, expanding the scope of detectable objects to tens of thousands. PromptDet [84] and DetPro [83] leverage prompt learning techniques to enhance the alignment between region visual feature and semantic feature. Additionally, some works unify object detection and phrase grounding tasks to pre-train a detector capable of open-vocabulary detection [19], [21], [87]. For example, GLIP [19] integrates image-language pre-training to align visual and textual data, improving object detection across diverse categories using text prompts. GroundingDINO [21] combines the DINO detector with grounded pre-training, enhancing open-set object detection by tight modality fusion between vision and language with large-scale datasets. The success of these approaches relies on two critical factors: 1) effective object proposal generation beyond training categories; and 2) large-scale image-text datasets that enable robust open-vocabulary classification capabilities.

The limited size of existing aerial image datasets, along with their distinct visual characteristics compared to natural images, leads to suboptimal generalization in region proposal generation for diverse categories. Consequently, open-vocabulary detection methods developed for natural images perform poorly on aerial images. To address the gap in open-vocabulary aerial detection, we introduce CastDet [36], the first approach designed specifically for this task, which tackles the unique challenges posed by aerial imagery through a student-multi-teacher self-learning paradigm. Following CastDet, a few studies further explore OVAD. For example, LAE-DINO [88] proposes a DINO-based detector with dynamic vocabulary construction and visual-guided text prompt learning to improve detection across diverse aerial categories. OVA-DETR [89] enhances feature extraction by leveraging image-text alignment with region-text contrastive loss and Bidirectional Vision-Language Fusion, particularly for small objects. However, none of these methods address the challenge of oriented object detection in aerial scenes. This paper aims to fill this blank and set a foundation for future research.

III. METHOD

We start by presenting the problem setting in Section IV-A). Next, we provide an overview of our CastDet framework in Section IV-B, which is composed of several key components: i) the student, a two-stage open-vocabulary detector, discussed in Section IV-B1; ii) the localization teacher, as detailed in Section IV-B2; and iii) the dynamic pseudo-label queue for maintaining high-confidence pseudo-labels, outlined in Section IV-B3. Finally, we elaborate on two open-vocabulary aerial object detection tasks: horizontal open-vocabulary detection in Section IV-C and oriented open-vocabulary detection in Section IV-D.

IV. METHODOLOGY

A. Preliminaries

Given an image $\mathbf{x} \in \mathbb{R}^{H \times W \times 3}$, our objective is to train a detector capable of detecting both base ($\mathcal{C}_{\text{base}}$) and novel ($\mathcal{C}_{\text{novel}}$) objects within the image. This task involves solving two subproblems: i) localize all objects with precise bounding boxes, where each box is represented by coordinates $b_i \in \mathbb{R}^4$ for horizontal objects, and $b_i \in \mathbb{R}^5$ for oriented objects; and ii) classify the i -th object with the category label $c_i \in \mathbb{R}^{\mathcal{C}_{\text{test}}}$, where $\mathcal{C}_{\text{test}} = \mathcal{C}_{\text{base}} \cup \mathcal{C}_{\text{novel}}$ and $\mathcal{C}_{\text{base}} \cap \mathcal{C}_{\text{novel}} = \emptyset$. During training, we utilize a labeled dataset $\mathcal{L} = \{(\mathbf{x}, \{(b, c)_k\}_i)\}_{i=1}^{|\mathcal{L}|}$ on a set of base categories, i.e., $c_k \in \mathbb{R}^{\mathcal{C}_{\text{base}}}$. Additionally, we incorporate an unlabeled dataset $\mathcal{U} = \{\mathbf{x}_i\}_{i=1}^{|\mathcal{U}|}$, which consists of images without bounding box annotations. The combined training dataset is represented as $\mathcal{D}_{\text{train}} = \mathcal{L} \cup \mathcal{U}$.

B. CLIP-Activated Student Teacher Framework

Architecture Overview. Fig. 3 illustrates an overview of our CastDet framework, which consists of a student model and two teacher models: a localization teacher and an external teacher. The student model is a two-stage object detection model (e.g., Faster R-CNN or Oriented RCNN) with a modified class-agnostic bounding box regression head (Φ_{LOC}) and a semantic classifier (Φ_{CLS}). It is trained on both labeled and unlabeled samples with pseudo boxes and category labels generated by the localization teacher and external teacher. The localization teacher is an exponential moving average (EMA) of the student model [70], which can aggregate the history information during the training iterations to obtain better and stable representations, ensuring the quality of the pseudo-labels. During training, the localization teacher generates two sets of pseudo-labels for the unlabeled images, one for training the student model and another with pseudo boxes serve as input to the external teacher for the pseudo category label generation. The external teacher is a frozen RemoteCLIP model [33], a vision-language fundamental model pre-trained on large-scale remote sensing image-text pairs, following the CLIP framework. It provides strong open-vocabulary classification ability by comparing the similarity between image and category embeddings. Additionally, a dynamic label queue is used to store the pseudo-labels generated by the external teacher, facilitating to maintain high-quality pseudo-labels and transfer data samples for the student model training.

1) *Student*: The student model is a two-stage object detector, such as Faster R-CNN and Oriented-RCNN, comprising a backbone encoder, a region proposal network (RPN), and a box head module:

$$\{\hat{y}_1, \dots, \hat{y}_n\} = \Phi_{\text{BOX}} \circ \Phi_{\text{RPN}} \circ \Phi_{\text{ENC}}(\mathbf{x})$$

To construct an open-vocabulary detector, we incorporate two key components into the box head: (1) a class-agnostic box regression head (Φ_{LOC}) to generate class-agnostic box coordinates, and (2) a semantic classifier head (Φ_{CLS}) to classify these objects beyond seen categories, i.e., open-vocabulary classification.

Class-agnostic box regression head (Φ_{LOC}) takes the RoI (Region of Interest) features as input and produces refined box

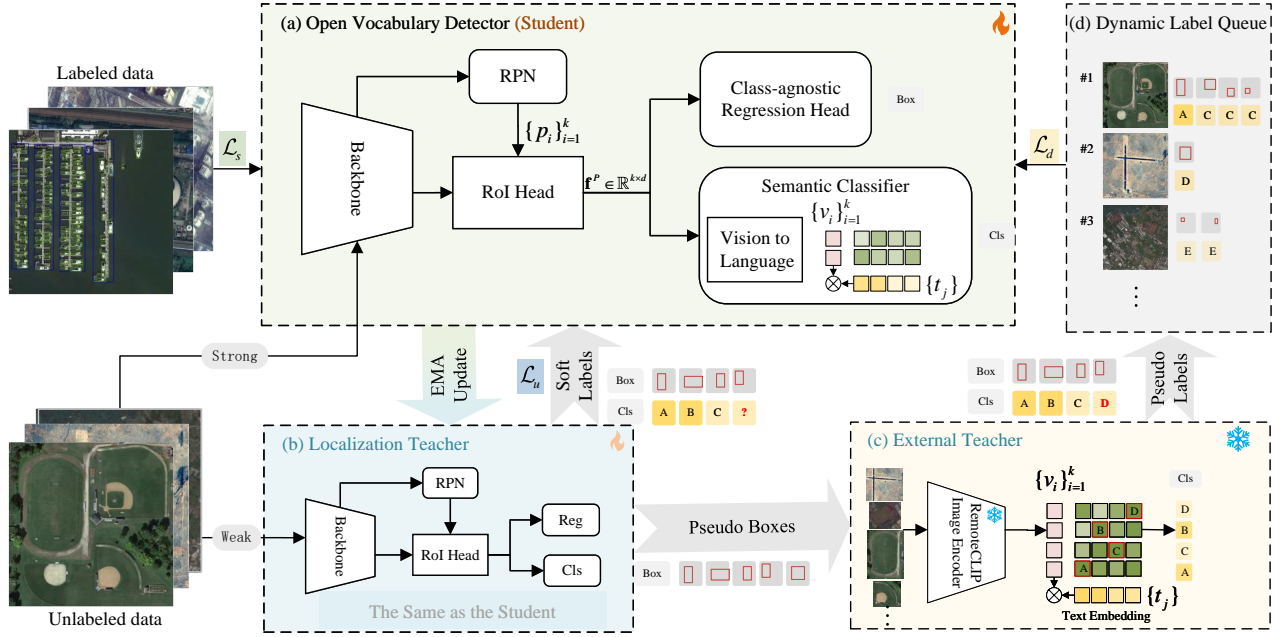


Fig. 3. Overall architecture of CastDet. In each training iteration, the data batch consists of three data flow: labeled data with annotations, unlabeled data, and data sampled from the dynamic label queue. The labeled images are directly used for the student network training (\mathcal{L}_s), while two sets of pseudo-labels of unlabeled data are predicted through the localization teacher and external teacher. One supervises the student (\mathcal{L}_u), and the other is pushed into the dynamic label queue. Simultaneously, samples are randomly selected from the dynamic label queue to enhance the student’s ability to detect novel objects (\mathcal{L}_d).

coordinates for each object. To handle a variable number of object categories, Φ_{LOC} shares parameters across all categories. Specifically, the regression box is represented as $b_i \in \mathbb{R}^k$ instead of $b_i \in \mathbb{R}^{k|\mathcal{C}_{\text{test}}|}$ for each box i , where $k \in \{4, 5\}$ is the dimension of the box. As described in [24], [84], this approach simplifies the model and enhances its versatility.

Semantic classifier head (Φ_{CLS}) is responsible for classifying RoI regions beyond a predefined set of categories. Following Detic [24], we employ semantic embeddings for category vocabularies as the weight of the last fully connected layer, allowing flexible category expansion. The semantic embeddings are generated by two steps: (1) filling the concept with a predefined prompt template “a photo of [category]”, and (2) encoding the text descriptions into semantic embeddings using the text encoder of RemoteCLIP.

$$t_j = \Phi_{\text{clip}}^{\text{text}} \circ \Phi_{\text{clip}}^{\text{tokenizer}}(\text{a photo of } [\text{category}]) \quad (1)$$

Given a set of RoI visual features $\{v_i\}_{i=1}^k$, the similarity score is calculated as

$$\hat{s}_{ij} = \frac{v_i^T \cdot t_j}{\tau \|v_i\| \cdot \|t_j\|}, \quad (2)$$

where τ is the temperature parameter that controls the range of the logits, optimized during training as a log parameterized multiplicative scalar as in [82].

2) *Localization Teacher*: The quality region proposals is fundamental for effectively detecting novel objects, as it directly impacts the subsequent box refinement and classification. However, as shown in Fig. 2(c), the RPN recall of novel categories in aerial images is significantly lower than that in natural images. To address this problem, we employ a robust teacher to generate better pseudo-boxes for the student

training. Our goal, then, is to derive a better teacher model from the student model without introducing additional training costs. A naive solution is to employ a frozen teacher model trained on base categories, but this is insufficient for open-vocabulary detection due to its lack of flexibility in learning novel categories. Thus, we opt for a continuously update mechanism, enabling the teacher to evolve and adapt to novel concepts, thereby enhancing its effectiveness in a broader detection context.

Exponential Moving Average. Inspired from [70], [90], we employ a momentum update strategy for the teacher model, that is, the teacher is updated by an exponential moving average of the student during training. Formally, denoting the parameters of the teacher model as θ' and those of the student model as θ . Only the parameters θ are updated by back-propagation, and θ' as a weighted average of successive weights of θ at each training iteration t :

$$\theta'_t = \alpha \theta'_{t-1} + (1 - \alpha) \theta_t \quad (3)$$

Here $\alpha \in [0, 1)$ is a momentum coefficient.

The momentum update described in Equ. (3) enhances the teacher model in several significant ways compared to a frozen teacher. 1) it enables the teacher to leverage unlabeled data effectively, enhancing the performance of the model with fewer annotated images; 2) it accumulates historical information of the student model without additional training costs, thereby obtaining better intermediate representations and more robust predictions [28], [70]; and 3) it facilitates on-line learning, allowing the model to continuously adapt and scale to an increasing number of novel concepts.

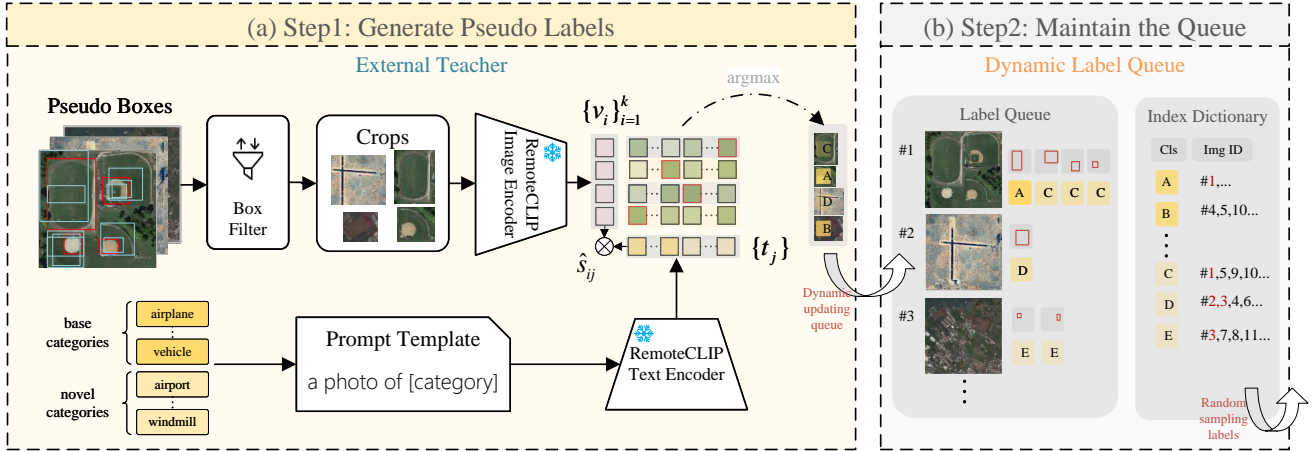


Fig. 4. Workflow of the dynamic label queue. **Step1**: filter certain high-quality proposal boxes generated by the localization teacher, and employ RemoteCLIP to classify corresponding cropped images as pseudo-labels. **Step2**: dynamically update the pseudo-labels into the queue, and randomly sample a batch of pseudo-labels for the student training.

Consistency Training. We apply consistency training [29], [30] that encourages the student to predict the same prediction as the teacher. Specifically, given an unlabeled image \mathbf{x} , it first go through weak augmentation and serve as input for the localization teacher to generate pseudo-labels. The pseudo-labels are then used to supervise the student model, which takes the same image with a strong augmentation as input. More formally, we define the prediction of the teacher model as $\hat{\mathbf{y}} = f(T'(\mathbf{x}), \theta')$. We then minimize the consistency cost J between $\hat{\mathbf{y}}$ and the predictions of the student model, i.e.,

$$J(\theta) = \mathcal{L}(f(T(\mathbf{x}), \theta), \hat{\mathbf{y}}) \quad (4)$$

where T and T' denote strong and weak augmentation, respectively.

3) *Dynamic pseudo-label Queue*: The dynamic label queue is responsible for storing, dynamically updating, and transferring pseudo-labels. At each training iteration, the localization teacher and external teacher generate high-quality pseudo-labels for the unlabeled images, which are then pushed into the label queue. Following this, a random batch of pseudo-labels is sampled from the dynamic queue for the student training, as illustrated in Fig. 4.

Generate pseudo-labels. The localization teacher take unlabeled images with weak augmentation $T'(\mathbf{x})$ as input, where the backbone first extracts features, the RPN then generates a set of proposals $\{p_i\}$ and extract RoI features $\mathbf{f}^P = \Phi_{\text{RPN}} \circ \Phi_{\text{ENC}}(T'(\mathbf{x}))$ of these proposals through RoI pooling. Subsequently, the class-agnostic regression branch predicts their refined coordinates $\{\hat{b}_i\}$. To improve the accuracy of pseudo-labels while reducing computational complexity, we use a box filter to select k candidates and obtain a set of image crops $\{\mathbf{x}_i^f\}_{i=1}^k$ by cropping the corresponding regions of the image. The category labels for these regions are then predicted by the RemoteCLIP.

For each cropped image \mathbf{x}_i^f , the visual feature v_i is computed via the visual encoder of the RemoteCLIP, denoted as $v_i = \Phi_{\text{clip}}^{\text{visual}}(\mathbf{x}_i^f)$. At the same time, text embeddings t_j corresponding to category descriptions are generated, as detailed in Sec. IV-B. The prediction probability for each

category j given the cropped image i is the softmax value for similarity between the visual feature and text embeddings:

$$\hat{p}_{ij} = \frac{e^{\hat{s}_{ij}}}{\sum_k e^{\hat{s}_{ik}}}, \quad (5)$$

where \hat{s}_{ij} is the similarity score, calculated by Equ (2).

We further apply a threshold p_0 to filter pseudo-labels, which is set relatively high to ensure the accuracy of pseudo-labels,

$$\hat{\mathbf{y}} = \{(\hat{b}_i, \hat{c}_i) | \hat{p}_i \geq p_0\}_{i=1}^k, \quad \hat{c}_i = \arg \max_j \hat{p}_{ij}, \quad \hat{p}_i = \max_j \hat{p}_{ij} \quad (6)$$

where \hat{p}_i , \hat{c}_i are the prediction score and category label, respectively. Finally, the image with its pseudo-labels $(\mathbf{x}, \hat{\mathbf{y}})$ is pushed into the dynamic label queue.

Maintain the Queue. As shown in Fig. 4(b), the dynamic label queue holds both image metadata and the associated pseudo-labels generated by the teacher models. Image metadata includes details such as the image index and file path, which are critical for tracking and retrieving images during the training process. Pseudo-labels, on the other hand, are comprised of annotations such as bounding boxes and class labels. To efficiently manage this queue, we utilize an index dictionary to store the mapping relationship between categories and image indexes, represented as $\{\text{cls_id}: \text{list}[\text{image_ids}]\}$. As new images are processed and pseudo-labels are generated, they are added to the queue, and the index dictionary is adjusted to include these updates. Additionally, images with pseudo-labels are sampled with a predefined probability based on the index dictionary, which are then used to train the student model.

This dynamic process allows the queue to progressively accumulate richer and more accurate pseudo-labels as the model iterates, with visualization results shown in Fig. 10. The continuous improvement benefits the entire system, enabling the student and localization teacher to learn from diverse, high-quality pseudo-labels.

C. Horizontal Open-vocabulary Detection

Horizontal object detection aims to detect all objects in a image and represent their location with horizontal bounding boxes, i.e., $b_i \in \mathbb{R}^4$. In theory, the detector can be any mainstream object detectors [26], [41], [43], here we use Faster R-CNN [26] as the base model to illustrate our method. To enable open-vocabulary detection, we incorporate external knowledge that may carry information about novel categories from unlabeled images into the training process. More specifically, the localization teacher first generates a set of box candidates, which are then filtered based on their confidence scores. Only those with high confidence are forwarded to the external teacher for category prediction. Subsequently, we leverage both unlabeled data with these high-quality pseudo-labels and labeled data to optimize the model via a hybrid training mechanism.

1) *Horizontal Box Selection Strategies*: The quality of pseudo-boxes is vital, as it directly affects the accuracy of the category labels generated by the external teacher, subsequently influencing the overall performance of the model. Given this context, we utilize several box confidence scores to filter high-quality pseudo boxes, including RPN, RJV and BJV Score, as shown in Fig. 5(a)~(c).

RPN Score. The RPN Score represents the confidence that a region contains an object. This strategy filters out boxes with low foreground confidence score, which is a common approach adopted by most OVD methods [23], [91]. As shown in Fig. 5(a), the RPN Score can be directly obtained from the region proposal network:

$$\text{RPN Score} = \Phi_{\text{RPN}}^{\text{score}} \circ \Phi_{\text{ENC}}(T'(\mathbf{x})) \quad (7)$$

Regression Jittering Variance (RJV). The RJV Score reflects the stability of object location predictions across M regression times. Regression jittering means we iteratively put the predicted box into the regression branch (Φ_{LOC}) for a more precise prediction. The RJV Score is defined as

$$\bar{\sigma}_i = \frac{1}{4} \sum_{k=1}^4 \frac{\sigma_{ik}^2}{(h_{-1}^2 + w_{-1}^2)} \quad (8)$$

where $\{\sigma_{ik}\}_{k=1}^4$ is the standard derivation of the coordinates (i.e., x_1, y_1, x_2, y_2) for the i -th set of regression boxes. The denominators h_{-1} and w_{-1} are the height and width of the last regression box, respectively, which serve to normalize the variance relative to the size of the box, thus making the score scale-invariant.

Box Jittering Variance (BJV). The BJV Score is employed to measure the stability of object location predictions across multiple jittered boxes. Box jittering involves introducing random noise around a predicted bounding box b_i to generate M jittered boxes. These jittered boxes are then processed by the box regression branch (Φ_{LOC}) to predict the refined bounding boxes, $\{\hat{b}_{i,j}\}$, where j ranges from 1 to M . The BJV is defined as follows

$$\bar{\sigma}_i = \frac{1}{4} \sum_{k=1}^4 \frac{\sigma_{ik}}{0.5(h_i + w_i)} \quad (9)$$

Here, $\{\sigma_{ik}\}_{k=1}^4$ represents the standard derivation of the coordinates (i.e., x_1, y_1, x_2, y_2) for the i -th set of refined

boxes. The terms h_i, w_i denote the mean height and width of the i -th boxes set, respectively [32].

2) *Hybrid Training*: We follow the student-teacher training mechanism. In each training iteration, three types of data flow are sampled from the training batch: The labeled data is directly used to supervise the student (\mathcal{L}_s). The unlabeled data is assigned pseudo-labels by the localization teacher and contributes to the unsupervised loss (\mathcal{L}_u). The pseudo-labeled data from the dynamic label queue encourages the model to discover novel objects (\mathcal{L}_d), as depicted in Fig. 3. Thus, the overall loss comprises three components:

$$\mathcal{L} = \alpha \mathcal{L}_s + \beta \mathcal{L}_u + \gamma \mathcal{L}_d, \quad (10)$$

where $\mathcal{L}_s, \mathcal{L}_u$ and \mathcal{L}_d represent the supervised loss for labeled images, unsupervised loss for unlabeled images with pseudos generated by the localization teacher, and unsupervised loss for images sampled from the dynamic label queue, respectively. The weights α, β and γ balance these loss components.

Labeled Data Flow. To achieve horizontal object detection, our approach adopts the architecture of Faster R-CNN, adapted to an open-vocabulary framework. In a typical processing batch, we receive a batch of labeled data $\{(\mathbf{x}_k, \{(b_i, c_i)\})\}$. The student model predicts the bounding box coordinates $\{\hat{b}_i\}$ and associated prediction scores $\{\hat{s}_i\}$ for these images, as depicted in Fig. 3(a). The supervised loss is then calculated as

$$\mathcal{L}_s = \frac{1}{N_b} \sum_{i=1}^{N_b} \mathcal{L}_{\text{cls}}(\hat{s}_i, c_i) + \frac{1}{N_b^{\text{fg}}} \sum_{i=1}^{N_b^{\text{fg}}} \mathcal{L}_{\text{reg}}(\hat{b}_i, b_i) \quad (11)$$

where \mathcal{L}_{cls} is the classification loss, calculated using Cross Entropy Loss. \mathcal{L}_{reg} is the box regression loss, calculated using L1 Loss. N_b denotes the total number of proposals generated by the model for each image, and N_b^{fg} represents the number of foreground proposals.

Unlabeled Data Flow. The unsupervised loss \mathcal{L}_u comprises two main components: the classification loss $\mathcal{L}_u^{\text{cls}}$ and the box regression loss $\mathcal{L}_u^{\text{reg}}$. During the initial training phases, the detector often struggles to correctly identify novel categories, leading to high rates of false negatives. To mitigate this issue without overly penalizing the model for incorrect background predictions, we employ a weighted mechanism for negative samples. The classification loss is defined as:

$$\mathcal{L}_u^{\text{cls}} = \frac{1}{N_b^{\text{fg}}} \sum_{i=1}^{N_b^{\text{fg}}} \mathcal{L}_{\text{cls}}(\hat{s}_i, \hat{c}_i) + \sum_{j=1}^{N_b^{\text{bg}}} w_j \mathcal{L}_{\text{cls}}(\hat{s}_j, \hat{c}_j) \quad (12)$$

where N_b^{bg} denotes the total number of background objects. The weight w_j for each background sample is determined by the normalized contribution of the background prediction score of the j -th candidate.

For training the box regression branch, we first apply the BJV score to filter candidates, as described in Sec. IV-B2. The regression loss is then defined as:

$$\mathcal{L}_u^{\text{reg}} = \frac{1}{N_b^{\text{fg}}} \sum_{i=1}^{N_b^{\text{fg}}} \mathcal{L}_{\text{reg}}(\hat{b}_i^{\text{fg}}, \hat{b}_i) \quad (13)$$

where \hat{b}_i^{fg} and \hat{b}_i denote the i -th predicted foreground box and the assigned pseudo box, respectively.

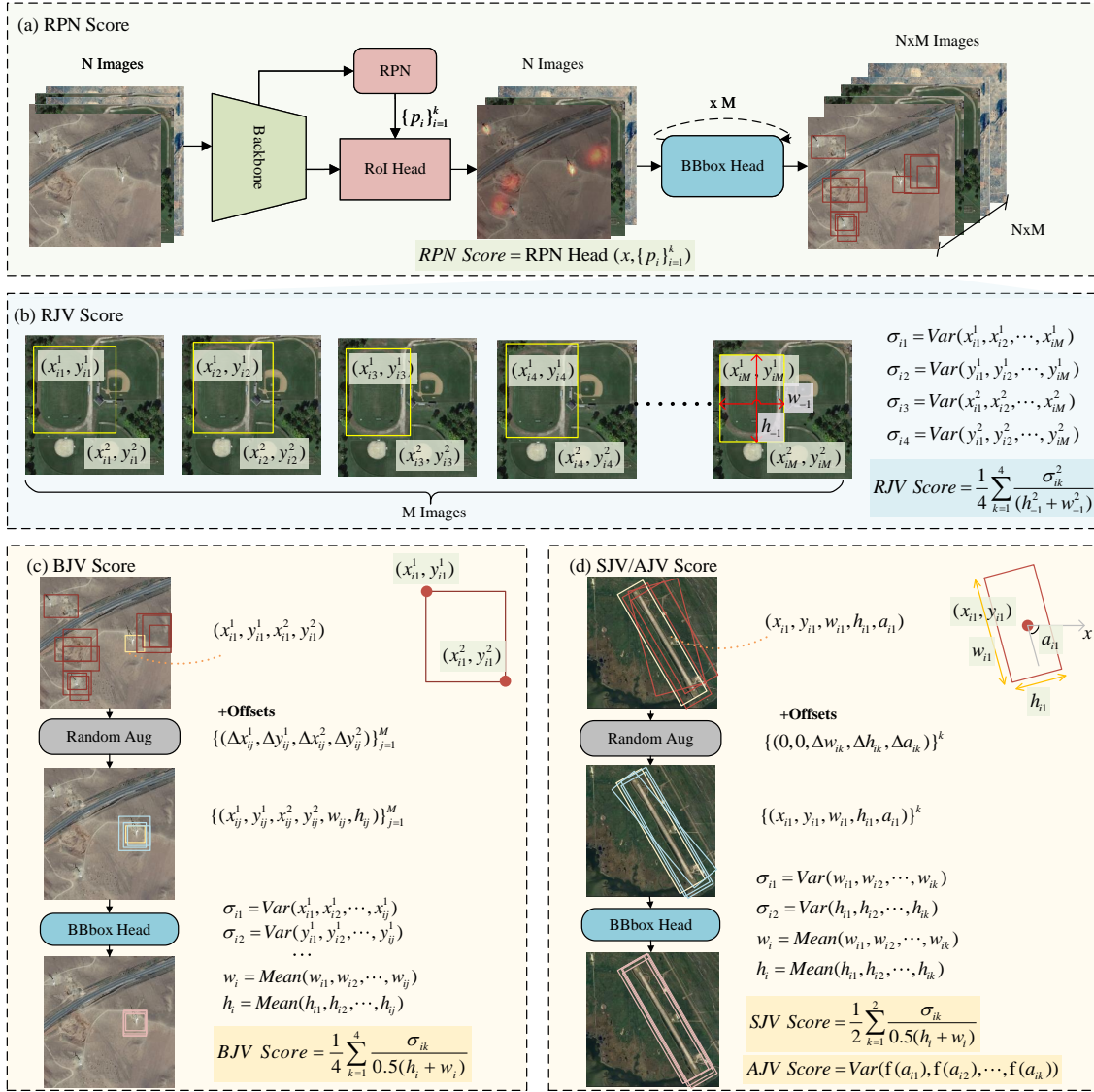


Fig. 5. Illustration for 5 types of box selection strategies, including horizontal box selection strategies: (a) RPN Score, (b) regression jittering score (RJV), (c) box jittering score (BJV); and oriented box selection strategies: (d) scale jittering score (SJV) and angle jittering score (AJV).

Queue Data Flow. To enhance the open-vocabulary capability, we randomly sample a batch of images from the dynamic label queue to train the student, see Sec. IV-B3. Like unsupervised loss, \mathcal{L}_d also includes two parts: $\mathcal{L}_d^{\text{cls}}$ and $\mathcal{L}_d^{\text{reg}}$. Since the localization teacher primarily guides the student in discovering and localizing objects, the $\mathcal{L}_d^{\text{reg}}$ is optional in this process. The classification loss is defined as follows:

$$\mathcal{L}_d^{\text{cls}} = \frac{1}{N_b^{\text{fg}}} \sum_{i=1}^{N_b^{\text{fg}}} \mathcal{L}_{\text{cls}}(\hat{s}_i, \hat{c}_i) + \sum_{j=1}^{N_b^{\text{bg}}} w_j \mathcal{L}_{\text{cls}}(\hat{s}_j, \hat{c}_j) \quad (14)$$

where w_j is a weighting factor, which balances the foreground and background loss.

D. Oriented Open-vocabulary Detection

Aerial objects often exhibit arbitrary orientation, the generic horizontal object detector cannot locate these oriented aerial

objects accurately. Therefore, we develop oriented open-vocabulary detector to address this problem. We utilize the Oriented R-CNN [27] framework as the base detector, which is capable of representing the objects with their oriented bounding boxes, each box is denoted by a 5-dimensional vector $b_i = (c_x, c_y, w, h, a)$, where (c_x, c_y) is the center coordinate of the box, w and h represent the width and height of the box, and a specifies the angle of rotation. The training objective are almost the same as horizontal detection training, as detailed in Sec. IV-C2. However, when generating oriented pseudo-labels, it is crucial to consider both the scale and orientation of the bounding boxes. This section describes two advanced strategies for selecting robust pseudo oriented boxes.

1) *Oriented Box Selection Strategies:* To filter robust pseudo boxes, we propose two types of rotated box selection strategies, box scale jittering variance (SJV) and angle jittering variance (AJV), which take scale and orientation of the objects into consideration, respectively.

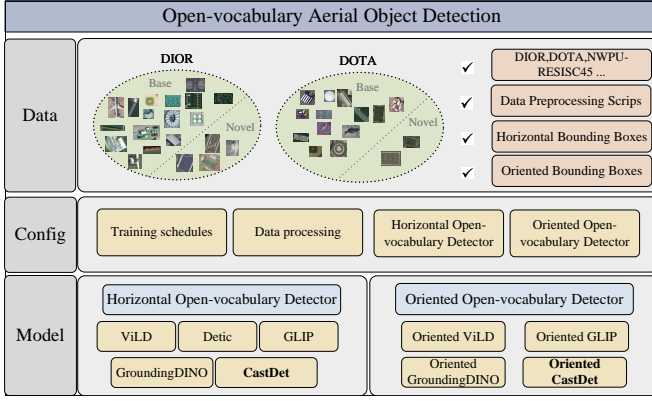


Fig. 6. Overview for open-vocabulary aerial detection framework.

Box Scale Jittering Variance (SJV). The SJV Score evaluates the scale stability across multiple noise instances. We first randomly add noise $(\Delta w, \Delta h, \Delta a)$ to box representations (w, h, a) , thus generate M jittered boxes. Here, we fix the center point (c_x, c_y) for each box. Then, the noised boxes are refined by the oriented regression branch. Finally, the scale jittering variance is calculated by

$$\bar{\sigma}_i = \frac{1}{2} \sum_{k=1}^2 \frac{\sigma_{ik}}{0.5(h_i + w_i)} \quad (15)$$

Here, σ_{ik} represents the standard deviation of the scale components (height and width), h_i and w_i are the mean height and width of the i -th set of jittered boxes.

Angle Jittering Variance (AJV). The AJV is used to access the stability of angle predictions, we first generate M jittered boxes follows the jittering strategy of SJV, and then compute angle jittering score by

$$\bar{\sigma}_i = \text{Var}(f(a_{i1}), f(a_{i2}), \dots, f(a_{ik})) \quad (16)$$

where a_{ij} denotes the angle of j -th box of i -th box set. The function $f(\cdot)$ denotes a function of the angle, which transform the angle values to better capture the variance in orientation, e.g., $\sin(\cdot)$ or Identity (\cdot) function.

V. EXPERIMENTS

A. Open-vocabulary Aerial Detection Benchmark

As shown in Fig. 6, we evaluate our approach and set the open-vocabulary aerial detection benchmark² on two typical aerial datasets: DIOR and DOTA. Following the setup of CastDet [36], we divide the classes into base (C_{base}) and novel (C_{novel}) categories. Specifically, we use 16 base classes and 4 novel classes for DIOR, 13 base classes and 2 novel classes for DOTA. During training, only the annotations for base categories are used. Our experiments cover two tasks: horizontal open-vocabulary detection and oriented open-vocabulary detection.

²The code is available at <https://github.com/lizzy8587/CastDet>.

1) *Datasets.*: To establish a robust benchmark, we evaluate our approach using several datasets:

DOTA [12] comprises 2,806 aerial images from different sensors and platforms with the resolution range from 800 to 4,000, annotated by 15 common categories. We crop the original images into $1,024 \times 1,024$ patches with an overlap of 200, and follow the guidelines in MMRotate [92] to merge the detection results of all patches for evaluation.

DIOR [11] provides a large collection of 23,463 images, each with a resolution of 800×800 . These images encompass 192,472 instances across 20 object classes. We extract 8,725 images to serve as unlabeled data. Evaluation is conducted on the test set.

VisDroneZSD [25] is a subset of DIOR [11], which contains 8,730 images for training and 3,337 images for testing. We follow the generalized zero-shot detection (GZSD) setting in VisDrone2023 Challenge to split the base/novel categories and train/test datasets of DIOR.

NWPU-RESISC45 [93] is a large-scale remote sensing classification dataset, covering 45 scene classes with 700 images in each class. NWPU-RESISC45 is used as extra weakly supervised training data for comparison experiment.

2) *Algorithms.*: For the open-vocabulary aerial detection task, we establish two types of OVAD benchmarks: HBB-based and OBB-based open-vocabulary detectors. Due to the absence of oriented open-vocabulary detection algorithms, we integrate orientation prediction into several well-established open-vocabulary detection frameworks. We involve significant improvements to these popular frameworks: ViLD [34], GLIP [19], and GroundingDINO [21]. These models are originally designed for horizontal object detection, which are adeptly transformed to predict the orientation of objects, resulting in the development of Oriented ViLD, Oriented GLIP, and Oriented GroundingDINO.

3) *Evaluation Metrics.*: In our evaluation, we adopt mean Average Precision (mAP), mean Average Recall (mAR), and Harmonic Mean (HM) as key metrics. The mAP and mAR metrics are computed at an Intersection over Union (IoU) threshold of 0.5. To provide a comprehensive evaluation, we follow the approach proposed in [25] and incorporate the Harmonic Mean. This metric provides a balanced perspective on overall performance, by evaluating results across base and novel categories. It can be applied to both mAP and mAR metrics, for example, using mAP as an illustration, HM is defined as follows:

$$\text{HM} = 2 \frac{\text{mAP}_{\text{base}} \cdot \text{mAP}_{\text{novel}}}{\text{mAP}_{\text{base}} + \text{mAP}_{\text{novel}}} \quad (17)$$

4) *Implementation Details.*: We implement our method with MMDetection 3.3.0 [94] and MMRotate 1.0.0 [92] toolbox. For horizontal open-vocabulary detection, we employ Faster R-CNN [26] with ResNet50-C4 [95] backbone as the base detector. The model is initialized by a pre-trained Soft Teacher [32] and R50-RemoteCLIP [33], followed by $10k$ iterations of training with a batch size of 12. For oriented object open-vocabulary detection, we utilize Oriented R-CNN [27] as the base detector. The model is initialize with a pre-trained Oriented R-CNN [27] and R50-RemoteCLIP, followed by

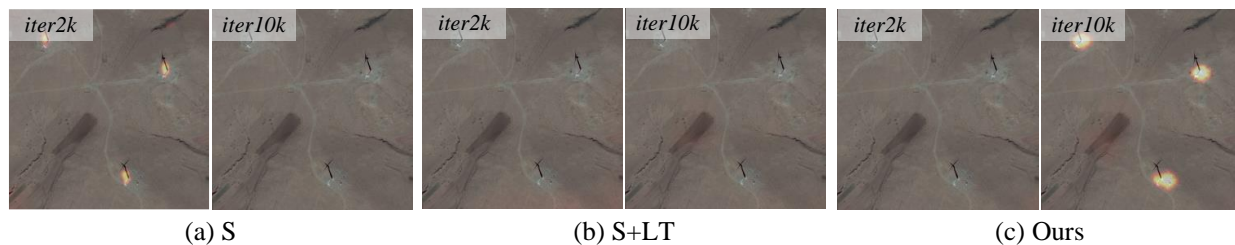


Fig. 7. Visualization of RPN foreground confidence during the training process. S, LT, ET denote student, localization teacher and external teacher, respectively.

TABLE I
EFFECTIVENESS OF HYBRID TRAINING IN ENHANCING NOVEL CATEGORY DISCOVERY. A COMPARATIVE ANALYSIS OF REGION PROPOSAL RECALL FOR DIFFERENT TRAINING STRATEGIES. S, LT, ET DENOTE THE STUDENT, LOCALIZATION TEACHER AND EXTERNAL TEACHER, RESPECTIVELY.

S	LT	ET	mAR	mAR _{base}	mAR _{novel}	HM	novel categories			
							airport	bball.ct	track.fld	windmill
✓			41.7	46.0	24.7	32.2	22.1	29.7	40.6	6.5
✓	✓		60.1	63.2	47.7	54.4	31.8	80.2	73.0	5.9
✓	✓	✓	63.6	62.2	69.1	65.5	72.1	91.8	71.3	41.3

10k iterations of training with a batch size of 8. We adopt Stochastic Gradient Descent (SGD) as the optimizer, using a learning rate of 0.01, with momentum and weight decay parameters set to 0.9 and 0.0001, respectively. To maintain high-confidence pseudo-labels, we set the RPN foreground threshold and prediction probability threshold p_0 relatively high at 0.95 and 0.8, respectively.

B. Ablation studies

a) Hybrid Training: To demonstrate the effectiveness of hybrid training in facilitating the discovery of novel categories, we evaluate the RPN recall of the detector across three training paradigms: supervised training (S), closed-vocabulary student-teacher semi-supervised training (S+LT), and our open-vocabulary hybrid training (S+LT+ET). For fairness, we employ class-agnostic recall, i.e., any object proposed by the RPN is considered successfully detected. As presented in Table I, our hybrid training strategy yields substantial improvements in RPN recall for novel categories compared to the semi-supervised approach (e.g., 69.1 vs. 47.7 mAR_{novel}).

Fig. 7 illustrates the visualization of RPN foreground confidence score map. The supervised pipeline, while initially capable of discovering novel objects, loses effectiveness in recognizing novel categories as the model focuses on refining classification and bounding box regression of base categories. The semi-supervised pipeline is limited to categories in the labeled dataset and lacks the ability to generalize to novel classes. In contrast, our method progressively enhances detection performance for novel categories, demonstrating a robust capability for open-vocabulary aerial detection.

b) H-Box Selection Strategy: We evaluate the effectiveness of different horizontal box selection metrics, including the RPN Score, RJV, and BJV, with the results summarized in Table II. The regression jittering strategy achieves a superior performance of 47.8% mAP_{novel}. As shown in Fig. 9(a)~(c), regression jittering exhibits a stronger correlation with both the

TABLE II
COMPARISON ON HORIZONTAL BOX SELECTION STRATEGIES.

Strategy	mAP	mAP _{base}	mAP _{novel}	HM
RPN Score	39.5	38.6	43.3	40.8
BJV Score	39.2	38.0	43.6	40.6
RJV Score	40.7	39.0	47.8	42.9

TABLE III
COMPARISON ON ORIENTED BOX SELECTION STRATEGIES.

Dataset	Strategy	mAP	mAP _{base}	mAP _{novel}	HM
DIOR	RPN Score	45.7	51.1	23.9	32.6
	AJV Score	45.7	51.1	24.2	32.8
	SJV Score	45.9	51.4	23.9	32.6
	AJV+SJV	45.9	51.3	24.3	33.0
DOTA	RPN Score	57.6	62.2	27.6	38.3
	AJV Score	57.4	61.6	30.2	40.6
	SJV Score	57.2	61.1	31.6	41.7
	AJV+SJV	58.1	61.7	34.9	44.6

TABLE IV
ABLATION ON DYNAMIC LABEL QUEUE.

Dynamic	Queue	mAP	mAP _{base}	mAP _{novel}	HM
✓		11.6	9.7	19.3	12.9
✓	✓	37.7	36.3	43.5	39.6
✓	✓	38.1	37.2	41.5	39.2
✓	✓	39.5	38.6	43.3	40.8

classification score and the IoU score, enabling the selection of more accurate pseudo-labels, which enhances the training process. The qualitative results of pseudo-labels under different box selection strategies are presented in Fig. 8.

c) R-Box Selection Strategy: We compare the effects of two oriented box selection strategies: SJV and AJV. Fig. 9(d)~(e) illustrates improved score correlation when employing SJV and AJV, which enhances the model training. Furthermore, Table III shows that using both AJV and SJV score yields better results, e.g., achieving 24.3% mAP_{novel} on

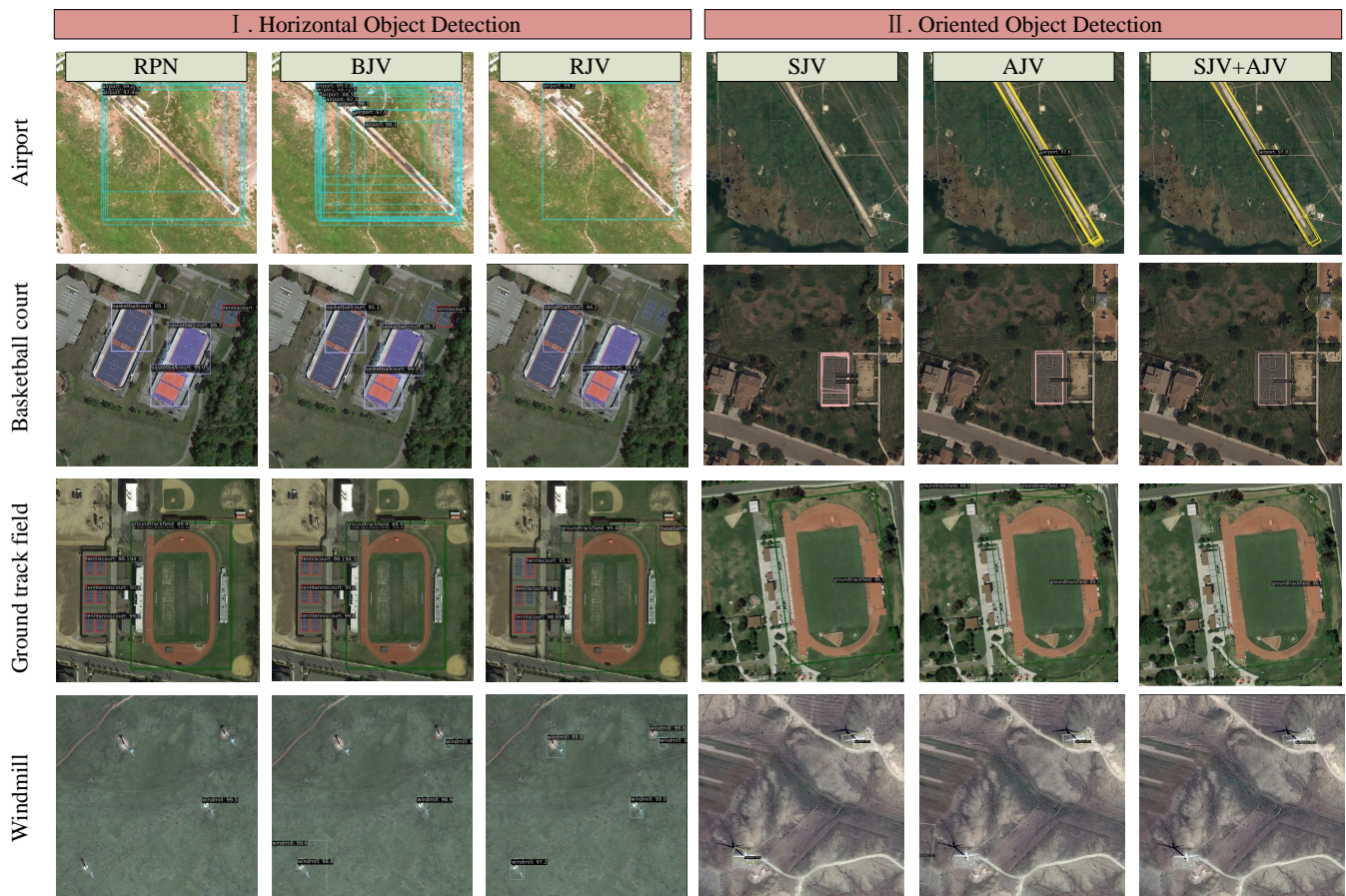


Fig. 8. Visualization of pseudo-labels of different box selection strategies on DIOR dataset. Left: horizontal pseudo-boxes selected by RPN, BJV and RJV score. Right: oriented pseudo-boxes selected by AJV and BJV score.

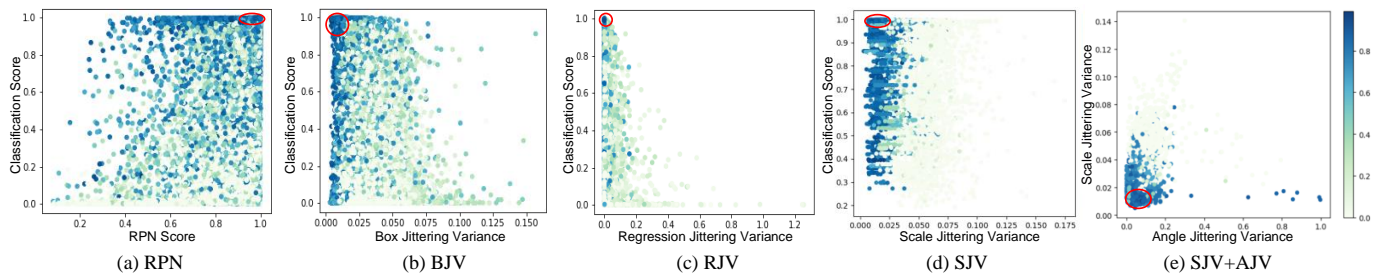


Fig. 9. Visualization of three types of box selection strategies. The figures shows the correlation among IoU, classification score, and (a) RPN score, (b) box-jittering variance, (c) regression-jittering variance, (d) oriented box scale-jittering variance, and (e) oriented angle-jitter variance respectively. Among them, IoU is represented by the color bar.

DIOR-R and 34.9% mAP_{novel} on DOTA-R. The visualization of selected pseudo-boxes is shown in Fig. 8.

d) Dynamic Label Queue: To demonstrate the effectiveness of dynamic label queue, we conduct experiments on whether to adopt a dynamic update strategy or whether to use a label queue for storing pseudo-labels Table IV shows substantial improvement achieved through applying dynamic updating strategy or using a label queue.

To further illustrate that the dynamic queue can obtain more accurate pseudo-labels, we analyze the pseudo-labels in the dynamic label queue across different training iterations. As illustrated in Fig. 10, with the model iterations, the precision-

recall (PR) curve expands outward (Fig. 10 (a)), and mAP_{50}^{novel} of pseudo-labels shows significant improvements (Fig. 10 (b)). This indicates that the dynamic label queue maintains richer and more accurate pseudo-labels as training progresses.

Moreover, Fig. 10(b) shows that the quality of pseudo-labels saturates at an mAP_{50}^{novel} around 16.9% after 4k iterations. This is expected, as a simple combination of the detector with RemoteCLIP is suboptimal for open-vocabulary detection. However, we can improve the mAP_{50}^{novel} to 43.3% by employing our hybrid training mechanism. Fig. 10(c) visualizes the pseudo-labels across different iterations. We can see that the model generates more accurate pseudo-labels (last row) and

TABLE V
ABLATION ON FRACTION OF LABELED DATA.

Label Fraction	mAP	mAP _{base}	mAP _{novel}	HM
34%	38.6	38.0	41.0	39.5
50%	38.8	37.7	43.4	40.4
100%	39.5	38.6	43.3	40.8

TABLE VI
ABLATION WITH DIFFERENT LOSS WEIGHTS DEFINED IN EQU. (10).

α	β	γ	mAP	mAP _{base}	mAP _{novel}	HM
1.0	1.0	1.0	62.6	67.7	29.6	41.2
2.0	1.0	1.0	59.1	64.2	26.0	37.1
1.0	2.0	1.0	58.1	61.7	34.9	44.6
1.0	1.0	2.0	60.0	65.0	27.7	38.9

TABLE VII
ABLATION WITH DIFFERENT BACKGROUND EMBEDDINGS.

BG Embedding	mAP	mAP _{base}	mAP _{novel}	HM
Zero	58.5	62.3	33.9	43.9
Normalize	58.4	62.1	34.2	44.2
Learnable	58.1	61.7	34.9	44.6

demonstrates an improved ability to discover novel objects (first two rows) as the training goes.

e) Label Fraction Experiments: To demonstrate that our model is well suited for the aerial scenario where labeled data is limited, we conduct label fraction experiments with 34%, 50% and full labeled data. Table V shows that even with only 34% of the original labeled data, the performance remains comparable, with only a minor reduction of 0.9% mAP.

f) Loss weights of \mathcal{L}_s , \mathcal{L}_u and \mathcal{L}_d : Table VI shows that $\alpha = 1.0$, $\beta = 2.0$ and $\gamma = 1.0$ could be better for novel categories.

g) Background Embeddings: We compare three common background embeddings: fixed all-zero embedding [35], fixed mean embedding [96], and learnable background embedding [97]. As shown in Table VII, the choice of background embedding has slight impact on our experimental results, with the learnable embedding showing better performance.

h) Prompt Templates: We evaluate four types of prompt templates, including T1: “[category]”, T2: “a [category]”, T3: “a satellite photo of [category]”, and T4: “a photo of [category]”. According to Table VIII, T4 is more suitable.

i) Function $f(\cdot)$ of AJV Score : Table IX compares two types of functions $f(\cdot)$ in Equ.(16), i.e., Identity(\cdot) and sin(\cdot). The results indicate that using sin(\cdot) function for angle transformation yields better performance. This improvement is attributed to the fact that the oriented box representation exhibits discontinuities at boundaries, and the sin(\cdot) function helps to smooth these discontinuities, resulting in more reliable variance estimates.

j) Cross evaluation: Some popular detectors for natural images, such as GroundingDINO and GLIP, underperform on novel aerial categories due to a lack of a robust strategy for discovering novel aerial objects. Thus, we provide them with pseudo-labels filtered by our box selection strategies, i.e., AJV and RJV. As shown in Table X, this leads to significant

TABLE VIII
ABLATION WITH DIFFERENT PROMPT TEMPLATES.

Template	mAP	mAP _{base}	mAP _{novel}	HM
T1	56.7	61.8	24.0	34.6
T2	55.9	60.3	27.3	37.6
T3	57.5	61.3	32.7	42.7
T4	58.1	61.7	34.9	44.6

TABLE IX
ABLATION ON FUNCTION $f(\cdot)$ OF AJV SCORE.

$f(\cdot)$	mAP	mAP _{base}	mAP _{novel}	HM
Identity(\cdot)	57.4	61.6	30.2	40.6
sin(\cdot)	59.1	63.3	31.2	41.8

TABLE X
BOOST GLIP/GROUNDINGDINO WITH OUR PSEUDO-LABELING STRATEGIES. †: USE PSEUDO-LABELS GENERATED BY OUR PSEUDO-LABELING STRATEGIES TO FINETUNE THE MODEL.

Method	mAP	mAP _{base}	mAP _{novel}	HM
GLIP	57.5	65.2	8.0	14.2
GroundingDINO	58.0	66.0	5.8	10.6
GLIP †	59.7	66.6	14.6	24.0
GroundingDINO †	47.0	51.5	17.6	26.3

improvements, e.g., 6.6% mAP_{novel} gains for GLIP and 11.8% mAP_{novel} gains for GroundingDINO, highlighting the effectiveness of our approach in bridging the gap between general object detection frameworks and the specialized requirements of aerial imagery.

C. Comparisons with state-of-the-art methods

1) Horizontal Object Detection:

a) Comparison with CLIPs: We compare our method with RemoteCLIP [33] under two settings: (1) using ground truth bounding boxes as proposals to measure open-vocabulary classification performance, and (2) employing proposals predicted by RPN to assess overall model performance. Table XI shows that CastDet outperforms RemoteCLIP in open-vocabulary classification, achieving an improvement from 37.6% to 47.3% mAP. Furthermore, CastDet shows significant performance gains when using RPN proposals, with mAP increasing from 11.6% to 38.1%. Additional experiments conducted on COCO [16] further validate the improvements achieved by our approach on natural images.

b) Comparison with SOTAs: In OVD, auxiliary weak supervision may be employed in various forms: **1)** leveraging both base and novel categories ($\mathcal{T}_{\text{novel}}$) with unlabeled images for knowledge distillation or pseudo-labeling, such as ViLD [34] and OV-DETR [85], which is consistent with our setting; and **2)** using image classification or image caption datasets (\mathcal{I}_{cls}) that contain novel concepts, such as Detic [24], etc [19], [21], [98], [99]. To support these approaches, we provide the NWPU-RESISC45 [93] classification dataset. We conduct experiments on DIOR and VisDroneZSD, as shown in Table XII. Our method outperforms the previous SOTA by 26.8% mAP_{novel}. Visualization results are presented in Fig. 11.

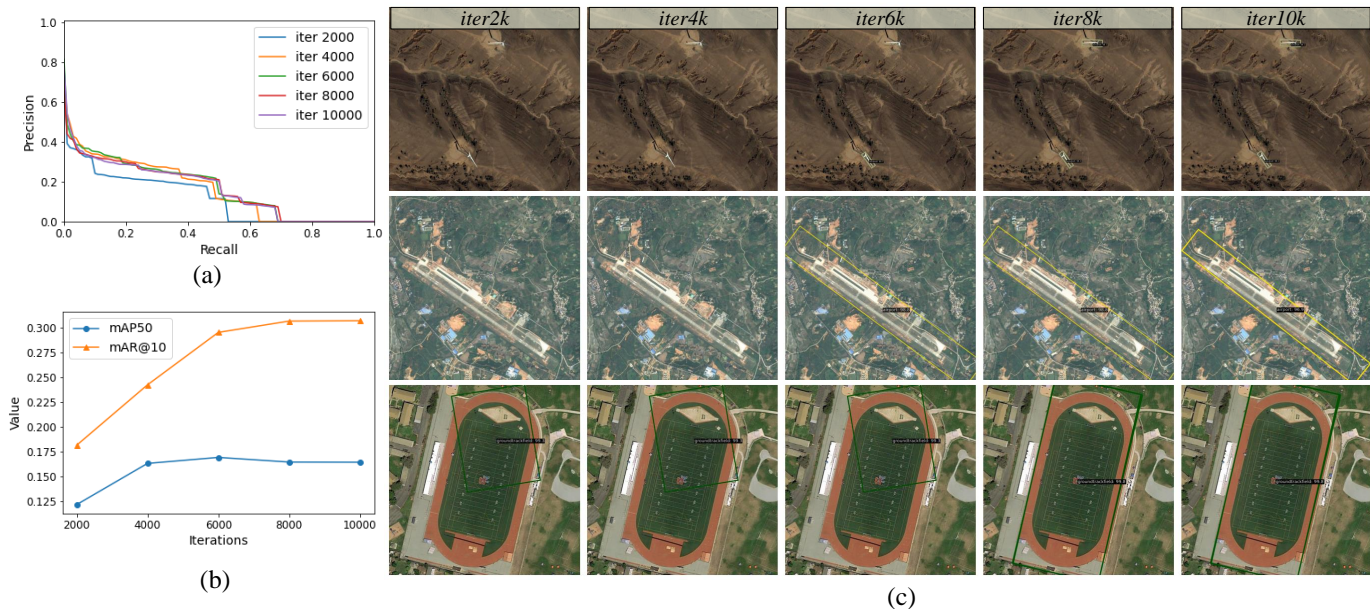


Fig. 10. Precision and recall statistics for novel categories of pseudo-labels in dynamic label queue. (a) Precision-recall curve for different iterations. (b) The mAP and mAR curve on iterations. (c) Visualization of pseudo-labels across different iterations.

TABLE XI
EVALUATION ON CLIPS (E.G., REMOTECLIP, CLIP) WITH GROUND-TRUTH (GT) OR RPN PROPOSALS.

Method	Proposal	VisDroneZSD				COCO			
		mAP	mAP _{base}	mAP _{novel}	HM	mAP	mAP _{base}	mAP _{novel}	HM
CLIP	GT	37.6	30.4	66.4	41.7	39.8	39.1	41.5	40.3
Ours	GT	47.3	46.6	49.9	48.2	51.8	55.5	41.4	47.4
CLIP	RPN	11.6	9.7	19.3	12.9	14.7	15.2	13.2	14.2
Ours	RPN	38.1	36.6	44.2	40.0	37.0	40.6	27.1	32.5

TABLE XII

HORIZONTAL OPEN-VOCABULARY DETECTION BENCHMARK ON DIOR DATASET. $\mathcal{T}_{\text{novel}}$ INDICATES WHETHER THE NOVEL CLASSES NEED TO BE PRE-KNOWN. \mathcal{I}_{cls} DENOTES WHETHER EXTRA CLASSIFICATION OR CAPTION DATASETS ARE REQUIRED DURING TRAINING. †: THE BEST RESULT ON THE ZERO-SHOT OBJECT DETECTION LEADERBOARD OF VISDRONE2023. ‡: THE RESULTS OF OUR OWN IMPLEMENTATION. THE SHORT NAMES FOR CATEGORIES ARE DEFINED AS: AIRPORT (APO), BASKETBALL COURT (BC), GROUND TRACK FIELD (GTF) AND WINDMILL (WM).

Dataset	Method	Detector	Backbone	$\mathcal{T}_{\text{novel}}$	\mathcal{I}_{cls}	APO	BC	GTF	WM	mAP	mAP _{base}	mAP _{novel}	HM	
VisDroneZSD	MultiModel	-	-	×	×	-	-	-	-	-	-	-	26.7†	
	ViLD‡ [34]	Faster R-CNN	R50	✓	×	9.1	11.8	26.9	9.1	25.6	28.5	14.2	19.0	
	OV-DETR [85]	Deformable DETR	R50	✓	×	29.1	20.5	26.8	5.2	28.7	30.8	20.6	24.7	
	Detic [24]	CenterNet2	R50	×	✓	2.0	2.2	15.0	0.0	16.8	19.8	4.8	7.7	
	GroundingDINO [21]	GroundingDINO	R50	×	✓	0.5	3.4	9.1	0.2	33.0	40.5	3.3	6.1	
	GLIP [19]	GLIP	Swin-T	×	✓	0.0	3.3	9.1	9.1	33.8	41.0	5.4	9.5	
	BARON [98]	Faster R-CNN	R50	×	✓	22.8	18.3	34.0	3.0	27.4	29.4	19.5	23.5	
	YOLO-World [99]	YOLOv8-M	YOLOv8-M	×	✓	0.0	20.1	13.7	0.0	32.9	39.1	8.5	13.9	
	CastDet (S)	Faster R-CNN	R50	×	×	57.3	75.6	33.3	23.2	36.4	33.7	47.4	39.4	
	CastDet (LT)	Faster R-CNN	R50	×	×	50.4	77.9	37.4	20.1	38.5	36.5	46.5	40.9	
	CastDet (S)	Faster R-CNN	R50	✓	×	37.3	77.6	34.6	16.3	35.2	33.6	41.5	37.1	
	CastDet (LT)	Faster R-CNN	R50	✓	×	47.5	78.3	43.3	16.0	40.5	39.0	46.3	42.3	
	DIOR	ViLD‡ [34]	Faster R-CNN	R50	✓	×	9.1	11.8	26.7	9.1	45.7	53.5	14.2	22.4
		OV-DETR [85]	Deformable DETR	R50	✓	×	29.1	19.7	25.6	5.2	54.0	62.6	19.9	30.2
Detic [24]		CenterNet2	R50	×	✓	0.7	2.2	11.2	0.0	36.9	45.3	3.5	6.5	
GroundingDINO [21]		GroundingDINO	R50	×	✓	0.3	3.3	9.1	0.2	57.3	70.8	3.2	6.2	
GLIP [19]		GLIP	Swin-T	×	✓	0.0	2.4	9.1	3.0	56.0	69.1	3.6	6.9	
BARON [98]		Faster R-CNN	R50	×	✓	14.1	16.6	30.4	0.1	50.9	59.8	15.3	24.4	
YOLO-World [99]		YOLOv8-M	YOLOv8-M	×	✓	0.0	19.8	12.2	0.0	57.7	70.2	8.0	14.4	
CastDet (S)		Faster R-CNN	R50	×	×	55.9	75.4	32.7	22.7	56.5	58.9	46.7	52.1	
CastDet (LT)		Faster R-CNN	R50	×	×	47.1	76.8	35.9	20.0	59.3	62.8	45.0	52.4	
CastDet (S)		Faster R-CNN	R50	✓	×	34.0	77.4	33.5	16.3	56.9	61.0	40.3	48.5	
CastDet (LT)	Faster R-CNN	R50	✓	×	45.4	78.2	41.3	15.9	61.6	65.7	<u>45.2</u>	53.6		

2) *Oriented Object Detection*: Given the absence of an oriented open-vocabulary detector, we adhere to the architectures used for horizontal detection and extend them for

oriented detection. We compare the proposed method with Oriented ViLD, Oriented GLIP and Oriented GroundingDINO. A benchmark for oriented open-vocabulary detection is es-



Fig. 11. Visualization of aerial open-vocabulary detection inference. Top: Open-vocabulary horizontal object detection results. Bottom: Open-vocabulary oriented object detection results. Novel categories in this figure include airport, basketball court, ground track field, and windmill.

TABLE XIII
ORIENTED OPEN-VOCABULARY DETECTION BENCHMARK ON DOTA-V1.0 DATASET. THE SHORT NAMES FOR CATEGORIES ARE DEFINED AS: PLANE (PL), BASEBALL DIAMOND (BD), GROUND TRACK FIELD (GTF) AND BASKETBALL COURT (BC).

Method	Detector	Backbone	$\mathcal{T}_{\text{novel}}$	\mathcal{I}_{cls}	PL	BD	...	GTF	BC	mAP	mAP _{base}	mAP _{novel}	HM
ViLD [34]	Faster-RCNN	R50	✓	✗	88.3	64.7	...	5.5	0.4	55.1	63.2	2.9	5.6
ViLD [34]	Oriented-RCNN	R50	✓	✗	89.2	<u>64.6</u>	...	4.7	0.4	59.0	67.7	2.5	4.8
GLIP [19]	GLIP	R50	✗	✓	86.8	<u>64.6</u>	...	9.8	6.1	57.5	65.2	8.0	14.2
GLIP [19]	GLIP	Swin-T	✗	✓	71.9	20.5	...	3.1	5.6	31.4	35.6	4.3	7.7
GroundingDINO [21]	GroundingDINO	R50	✗	✓	88.4	53.2	...	3.0	0.7	53.1	61.0	1.9	3.6
GroundingDINO [21]	GroundingDINO	Swin-T	✗	✓	88.1	58.8	...	0.7	10.8	<u>58.0</u>	66.0	5.8	10.6
CastDet (S)	Faster-RCNN	R50	✓	✗	88.5	42.0	...	30.5	25.7	52.8	56.6	28.1	37.6
CastDet (LT)	Faster-RCNN	R50	✓	✗	88.5	51.2	...	27.6	30.7	56.1	60.3	29.2	39.3
CastDet (S)	Oriented-RCNN	R50	✓	✗	88.9	50.3	...	<u>32.4</u>	<u>33.3</u>	55.8	59.3	<u>32.8</u>	<u>42.3</u>
CastDet (LT)	Oriented-RCNN	R50	✓	✗	88.6	57.5	...	34.2	37.7	57.3	60.6	36.0	45.1

TABLE XIV
ORIENTED OPEN-VOCABULARY DETECTION BENCHMARK ON DIOR DATASET. THE SHORT NAMES FOR CATEGORIES ARE DEFINED AS: AIRPLANE (APL), AIRPORT (APO), BASKETBALL COURT (BC), GROUND TRACK FIELD (GTF) AND WINDMILL (WM).

Method	Detector	Backbone	$\mathcal{T}_{\text{novel}}$	\mathcal{I}_{cls}	APL	...	APO	BC	GTF	WM	mAP	mAP _{base}	mAP _{novel}	HM
ViLD [34]	Faster-RCNN	R50	✓	✗	52.3	...	1.1	2.1	27.2	6.1	37.5	44.6	9.1	15.2
ViLD [34]	Oriented-RCNN	R50	✓	✗	53.6	...	0.2	2.3	16.3	9.1	39.3	47.4	7.0	12.2
GLIP [19]	GLIP	R50	✗	✓	43.3	...	0.1	1.6	20.2	0.0	39.4	47.9	5.5	9.8
GLIP [19]	GLIP	Swin-T	✗	✓	33.3	...	0.1	2.6	13.8	0.0	28.7	34.8	4.1	7.4
GroundingDINO [21]	GroundingDINO	R50	✗	✓	43.7	...	0.1	0.4	10.8	0.0	39.5	48.7	2.8	5.3
GroundingDINO [21]	GroundingDINO	Swin-T	✗	✓	48.0	...	0.9	7.3	8.4	0.1	45.0	55.3	4.2	7.8
CastDet (S)	Faster-RCNN	R50	✓	✗	52.9	...	1.7	51.1	26.8	1.6	40.3	45.3	20.3	28.0
CastDet (LT)	Faster-RCNN	R50	✓	✗	53.9	...	9.1	45.4	27.2	2.8	44.3	50.1	21.1	29.7
CastDet (S)	Oriented-RCNN	R50	✓	✗	53.2	...	9.8	41.5	27.3	9.1	42.8	48.0	21.9	30.1
CastDet (LT)	Oriented-RCNN	R50	✓	✗	<u>53.8</u>	...	<u>9.2</u>	49.8	29.3	9.1	45.9	51.3	<u>24.3</u>	33.0

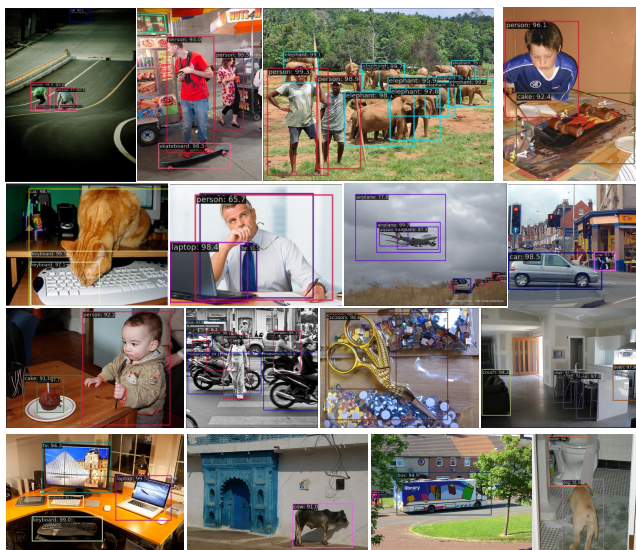


Fig. 12. Visualization of open-vocabulary COCO inference. Novel categories in this figure include skateboard, elephant, cake, keyboard, cat, tie, airplane, cow, bus, scissors, couch, and dog.

TABLE XV

RESULTS ON OPEN-VOCABULARY COCO. †: RESULTS QUOTED FROM [81]. ‡: THE RESULTS OF OUR OWN IMPLEMENTATION, UNDER THE SAME EXPERIMENTAL SETUP AS OURS. *: RESULTS QUOTED FROM THE ORIGINAL PAPER.

	mAP _{novel}	mAP _{base}	mAP50 _{all}	HM
Mask R-CNN [40]	-	51.4	-	-
WSDDN [100]†	19.7	19.6	19.6	19.6
Cap2Det [101]†	20.3	20.1	20.1	20.2
OVR-CNN [81]*	22.8	46.0	39.9	30.5
Detic [24]*	24.1	52.0	44.7	32.9
ViLD [34]‡	12.9	38.8	32.0	19.3
PromptDet [84]*	26.6	59.1	50.6	36.7
CastDet (Ours)	30.3	47.4	42.9	37.0

tablished on two oriented datasets: DOTA-v1.0 and DIOR, with results shown in Table XIII and Table XIV. Our method achieves competitive performance, e.g., 36.0% mAP_{novel} on DOTA-v1.0 and 24.3% mAP_{novel} on DIOR. Fig. 11 shows the visualization results.

3) *Natural Images Open-vocabulary Detection*: To further assess the effectiveness of the proposed method beyond aerial imagery, we extend our evaluations to include the COCO dataset. As shown in Table XV, our method achieves impressive results in novel category detection, reaching a 30.3% mAP_{novel}. The qualitative results are shown in Fig. 12.

VI. CONCLUSION

In this paper, we address open-vocabulary aerial object detection, tackling challenges such as limited annotated data and unique characteristics in aerial scenarios. We present Cast-Det, a CLIP-activated student-teacher detector that supports horizontal and oriented detection. By incorporating a flexible student-(multi)teacher self-learning approach, a dynamic label queue, and several box selection strategies tailored for aerial scenarios, our method effectively bridges the gap between general open-vocabulary detection and the specific needs of aerial

imagery. We conduct experiments on several aerial datasets, such as DIOR and DOTA, achieving significant performance improvements. To the best of our knowledge, this marks the first effort in open-vocabulary aerial detection. We aspire for the proposed techniques and the established benchmark to lay a solid foundation for future research in this area.

ACKNOWLEDGMENTS

This work was supported by the National Natural Science Foundation of China (62071333), Fundamental Research Funds for the Central Universities (22120220654), Tongji University national artificial intelligence production-education integration innovation project, and the Science and Technology on Near-Surface Detection Laboratory (6142414221606).

REFERENCES

- [1] T. Zhao and R. Nevatia, "Car detection in low resolution aerial images," *Image and vision computing*, vol. 21, no. 8, pp. 693–703, 2003.
- [2] V. Reilly, H. Idrees, and M. Shah, "Detection and tracking of large number of targets in wide area surveillance," in *Computer Vision—ECCV 2010: 11th European Conference on Computer Vision, Heraklion, Crete, Greece, September 5–11, 2010, Proceedings, Part III 11*. Springer, 2010, pp. 186–199.
- [3] E. J. Sadgrove, G. Falzon, D. Miron, and D. W. Lamb, "Real-time object detection in agricultural/remote environments using the multiple-expert colour feature extreme learning machine (mec-elm)," *Computers in Industry*, vol. 98, pp. 183–191, 2018.
- [4] L. W. Sommer, T. Schuchert, and J. Beyerer, "Fast deep vehicle detection in aerial images," in *2017 IEEE Winter Conference on Applications of Computer Vision (WACV)*, 2017, pp. 311–319.
- [5] J. Ding, N. Xue, Y. Long, G.-S. Xia, and Q. Lu, "Learning roi transformer for oriented object detection in aerial images," in *Proceedings of the IEEE/CVF Conference on Computer Vision and Pattern Recognition*, 2019, pp. 2849–2858.
- [6] X. Yang, J. Yan, Z. Feng, and T. He, "R3det: Refined single-stage detector with feature refinement for rotating object," in *Proceedings of the AAAI conference on artificial intelligence*, vol. 35, no. 4, 2021, pp. 3163–3171.
- [7] W. Qian, X. Yang, S. Peng, X. Zhang, and J. Yan, "Rsdet++: Point-based modulated loss for more accurate rotated object detection," *IEEE Transactions on Circuits and Systems for Video Technology*, vol. 32, no. 11, pp. 7869–7879, 2022.
- [8] X. Yang, J. Yang, J. Yan, Y. Zhang, T. Zhang, Z. Guo, X. Sun, and K. Fu, "Scrdet: Towards more robust detection for small, cluttered and rotated objects," in *Proceedings of the IEEE/CVF international conference on computer vision*, 2019, pp. 8232–8241.
- [9] F. Yang, H. Fan, P. Chu, E. Blasch, and H. Ling, "Clustered object detection in aerial images," in *Proceedings of the IEEE/CVF international conference on computer vision*, 2019, pp. 8311–8320.
- [10] G. Cheng, P. Zhou, and J. Han, "Learning rotation-invariant convolutional neural networks for object detection in vhr optical remote sensing images," *IEEE Transactions on Geoscience and Remote Sensing*, vol. 54, no. 12, pp. 7405–7415, 2016.
- [11] K. Li, G. Wan, G. Cheng, L. Meng, and J. Han, "Object detection in optical remote sensing images: A survey and a new benchmark," *ISPRS journal of photogrammetry and remote sensing*, vol. 159, pp. 296–307, 2020.
- [12] G.-S. Xia, X. Bai, J. Ding, Z. Zhu, S. Belongie, J. Luo, M. Datcu, M. Pelillo, and L. Zhang, "Dota: A large-scale dataset for object detection in aerial images," in *2018 IEEE/CVF Conference on Computer Vision and Pattern Recognition*, 2018, pp. 3974–3983.
- [13] Z. Zou and Z. Shi, "Random access memories: A new paradigm for target detection in high resolution aerial remote sensing images," *IEEE Transactions on Image Processing*, vol. 27, no. 3, pp. 1100–1111, 2017.
- [14] P. Zhu, L. Wen, D. Du, X. Bian, H. Fan, Q. Hu, and H. Ling, "Detection and tracking meet drones challenge," *IEEE Transactions on Pattern Analysis and Machine Intelligence*, vol. 44, no. 11, pp. 7380–7399, 2021.

- [15] Y. Li, L. Wang, T. Wang, X. Yang, J. Luo, Q. Wang, Y. Deng, W. Wang, X. Sun, H. Li *et al.*, “Star: A first-ever dataset and a large-scale benchmark for scene graph generation in large-size satellite imagery,” *arXiv preprint arXiv:2406.09410*, 2024.
- [16] T.-Y. Lin, M. Maire, S. Belongie, J. Hays, P. Perona, D. Ramanan, P. Dollár, and C. L. Zitnick, “Microsoft coco: Common objects in context,” in *Computer Vision—ECCV 2014: 13th European Conference, Zurich, Switzerland, September 6–12, 2014, Proceedings, Part V 13*. Springer, 2014, pp. 740–755.
- [17] A. Gupta, P. Dollar, and R. Girshick, “Lvis: A dataset for large vocabulary instance segmentation,” in *Proceedings of the IEEE/CVF conference on computer vision and pattern recognition*, 2019, pp. 5356–5364.
- [18] J. Deng, W. Dong, R. Socher, L.-J. Li, K. Li, and L. Fei-Fei, “Imagenet: A large-scale hierarchical image database,” in *2009 IEEE Conference on Computer Vision and Pattern Recognition*, 2009, pp. 248–255.
- [19] L. H. Li, P. Zhang, H. Zhang, J. Yang, C. Li, Y. Zhong, L. Wang, L. Yuan, L. Zhang, J.-N. Hwang, K.-W. Chang, and J. Gao, “Grounded language-image pre-training,” in *2022 IEEE/CVF Conference on Computer Vision and Pattern Recognition (CVPR)*, 2022, pp. 10 955–10 965.
- [20] L. Yao, J. Han, Y. Wen, X. Liang, D. Xu, W. Zhang, Z. Li, C. Xu, and H. Xu, “Detclip: Dictionary-enriched visual-concept paralleled pre-training for open-world detection,” *Advances in Neural Information Processing Systems*, vol. 35, pp. 9125–9138, 2022.
- [21] S. Liu, Z. Zeng, T. Ren, F. Li, H. Zhang, J. Yang, C. Li, J. Yang, H. Su, J. Zhu *et al.*, “Grounding dino: Marrying dino with grounded pre-training for open-set object detection,” *arXiv preprint arXiv:2303.05499*, 2023.
- [22] X. Zhang, T. Zhang, G. Wang, P. Zhu, X. Tang, X. Jia, and L. Jiao, “Remote sensing object detection meets deep learning: A metareview of challenges and advances,” *IEEE Geoscience and Remote Sensing Magazine*, vol. 11, no. 4, pp. 8–44, 2023.
- [23] K. Chen, X. Jiang, Y. Hu, X. Tang, Y. Gao, J. Chen, and W. Xie, “Ovarnet: Towards open-vocabulary object attribute recognition,” in *Proceedings of the IEEE/CVF Conference on Computer Vision and Pattern Recognition*, 2023, pp. 23 518–23 527.
- [24] X. Zhou, R. Girdhar, A. Joulin, P. Krähenbühl, and I. Misra, “Detecting twenty-thousand classes using image-level supervision,” in *European Conference on Computer Vision*. Springer, 2022, pp. 350–368.
- [25] A. team at Lab of Machine Learning and D. Mining, “Zero-shot object detection challenge,” 2023, <http://aiskyeye.com/challenge-2023/zero-shot-object-detection/>, Last accessed on 2023-11-09.
- [26] S. Ren, K. He, R. Girshick, and J. Sun, “Faster r-cnn: Towards real-time object detection with region proposal networks,” *Advances in neural information processing systems*, vol. 28, 2015.
- [27] X. Xie, G. Cheng, J. Wang, X. Yao, and J. Han, “Oriented r-cnn for object detection,” in *Proceedings of the IEEE/CVF International Conference on Computer Vision (ICCV)*, October 2021, pp. 3520–3529.
- [28] Y.-C. Liu, C.-Y. Ma, Z. He, C.-W. Kuo, K. Chen, P. Zhang, B. Wu, Z. Kira, and P. Vajda, “Unbiased teacher for semi-supervised object detection,” *arXiv preprint arXiv:2102.09480*, 2021.
- [29] J. Jeong, S. Lee, J. Kim, and N. Kwak, “Consistency-based semi-supervised learning for object detection,” *Advances in neural information processing systems*, vol. 32, 2019.
- [30] K. Sohn, Z. Zhang, C.-L. Li, H. Zhang, C.-Y. Lee, and T. Pfister, “A simple semi-supervised learning framework for object detection,” *arXiv preprint arXiv:2005.04757*, 2020.
- [31] Q. Zhou, C. Yu, Z. Wang, Q. Qian, and H. Li, “Instant-teaching: An end-to-end semi-supervised object detection framework,” in *Proceedings of the IEEE/CVF conference on computer vision and pattern recognition*, 2021, pp. 4081–4090.
- [32] M. Xu, Z. Zhang, H. Hu, J. Wang, L. Wang, F. Wei, X. Bai, and Z. Liu, “End-to-end semi-supervised object detection with soft teacher,” in *Proceedings of the IEEE/CVF International Conference on Computer Vision*, 2021, pp. 3060–3069.
- [33] F. Liu, D. Chen, Z. Guan, X. Zhou, J. Zhu, and J. Zhou, “Remoteflip: A vision language foundation model for remote sensing,” *arXiv preprint arXiv:2306.11029*, 2023.
- [34] X. Gu, T.-Y. Lin, W. Kuo, and Y. Cui, “Open-vocabulary object detection via vision and language knowledge distillation,” *arXiv preprint arXiv:2104.13921*, 2021.
- [35] Y. Zhong, J. Yang, P. Zhang, C. Li, N. Codella, L. H. Li, L. Zhou, X. Dai, L. Yuan, Y. Li *et al.*, “Regionclip: Region-based language-image pretraining,” in *Proceedings of the IEEE/CVF Conference on Computer Vision and Pattern Recognition*, 2022, pp. 16 793–16 803.
- [36] Y. Li, W. Guo, X. Yang, N. Liao, D. He, J. Zhou, and W. Yu, “Toward open vocabulary aerial object detection with clip-activated student-teacher learning,” 2024. [Online]. Available: <https://arxiv.org/abs/2311.11646>
- [37] R. Girshick, J. Donahue, T. Darrell, and J. Malik, “Rich feature hierarchies for accurate object detection and semantic segmentation,” in *Proceedings of the IEEE conference on computer vision and pattern recognition*, 2014, pp. 580–587.
- [38] R. Girshick, “Fast r-cnn,” in *Proceedings of the IEEE international conference on computer vision*, 2015, pp. 1440–1448.
- [39] Z. Cai and N. Vasconcelos, “Cascade r-cnn: Delving into high quality object detection,” in *Proceedings of the IEEE conference on computer vision and pattern recognition*, 2018, pp. 6154–6162.
- [40] K. He, G. Gkioxari, P. Dollár, and R. Girshick, “Mask r-cnn,” in *Proceedings of the IEEE international conference on computer vision*, 2017, pp. 2961–2969.
- [41] J. Redmon, S. Divvala, R. Girshick, and A. Farhadi, “You only look once: Unified, real-time object detection,” in *Proceedings of the IEEE conference on computer vision and pattern recognition*, 2016, pp. 779–788.
- [42] W. Liu, D. Anguelov, D. Erhan, C. Szegedy, S. Reed, C.-Y. Fu, and A. C. Berg, “Ssd: Single shot multibox detector,” in *Computer Vision—ECCV 2016: 14th European Conference, Amsterdam, The Netherlands, October 11–14, 2016, Proceedings, Part I 14*. Springer, 2016, pp. 21–37.
- [43] T.-Y. Lin, P. Goyal, R. Girshick, K. He, and P. Dollár, “Focal loss for dense object detection,” in *Proceedings of the IEEE international conference on computer vision*, 2017, pp. 2980–2988.
- [44] H. Law and J. Deng, “Cornernet: Detecting objects as paired key-points,” in *Proceedings of the European conference on computer vision (ECCV)*, 2018, pp. 734–750.
- [45] Z. Tian, C. Shen, H. Chen, and T. He, “Fcos: Fully convolutional one-stage object detection,” in *Proceedings of the IEEE/CVF international conference on computer vision*, 2019, pp. 9627–9636.
- [46] X. Zhou, D. Wang, and P. Krähenbühl, “Objects as points,” *arXiv preprint arXiv:1904.07850*, 2019.
- [47] N. Carion, F. Massa, G. Synnaeve, N. Usunier, A. Kirillov, and S. Zagoruyko, “End-to-end object detection with transformers,” in *European conference on computer vision*. Springer, 2020, pp. 213–229.
- [48] J. Han, J. Ding, N. Xue, and G.-S. Xia, “Redet: A rotation-equivariant detector for aerial object detection,” in *Proceedings of the IEEE/CVF Conference on Computer Vision and Pattern Recognition (CVPR)*, June 2021, pp. 2786–2795.
- [49] Y. Li, J. Luo, Y. Zhang, Y. Tan, J.-G. Yu, and S. Bai, “Learning to holistically detect bridges from large-size vhr remote sensing imagery,” *IEEE Transactions on Pattern Analysis and Machine Intelligence*, pp. 1–18, 2024.
- [50] Z. Zheng, Y. Zhong, A. Ma, X. Han, J. Zhao, Y. Liu, and L. Zhang, “Hynet: Hyper-scale object detection network framework for multiple spatial resolution remote sensing imagery,” *ISPRS Journal of Photogrammetry and Remote Sensing*, vol. 166, pp. 1–14, 2020. [Online]. Available: <https://www.sciencedirect.com/science/article/pii/S0924271620301167>
- [51] X. Yang, H. Sun, K. Fu, J. Yang, X. Sun, M. Yan, and Z. Guo, “Automatic ship detection in remote sensing images from google earth of complex scenes based on multiscale rotation dense feature pyramid networks,” *Remote. Sens.*, vol. 10, p. 132, 2018. [Online]. Available: <https://api.semanticscholar.org/CorpusID:2027880>
- [52] C. Xu, J. Wang, W. Yang, H. Yu, L. Yu, and G.-S. Xia, “Rfla: Gaussian receptive field based label assignment for tiny object detection,” in *European Conference on Computer Vision*. Springer, 2022, pp. 526–543.
- [53] R. Zhang, J. Yao, K. Zhang, C. Feng, and J. Zhang, “S-cnn-based ship detection from high-resolution remote sensing images,” *The International Archives of the Photogrammetry, Remote Sensing and Spatial Information Sciences*, vol. 41, pp. 423–430, 2016.
- [54] M. Kang, X. Leng, Z. Lin, and K. Ji, “A modified faster r-cnn based on cfar algorithm for sar ship detection,” in *2017 International Workshop on Remote Sensing with Intelligent Processing (RSIP)*. IEEE, 2017, pp. 1–4.
- [55] Y. Liu, M.-h. Zhang, P. Xu, and Z.-w. Guo, “Sar ship detection using sea-land segmentation-based convolutional neural network,” in *2017 international workshop on remote sensing with intelligent processing (RSIP)*. IEEE, 2017, pp. 1–4.
- [56] S. M. Azimi, E. Vig, R. Bahmanyar, M. Körner, and P. Reinartz, “Towards multi-class object detection in unconstrained remote sensing imagery,” in *Asian conference on computer vision*. Springer, 2018, pp. 150–165.

- [57] X. Yang and J. Yan, "On the arbitrary-oriented object detection: Classification based approaches revisited," *International Journal of Computer Vision*, vol. 130, no. 5, pp. 1340–1365, 2022.
- [58] X. Yang, L. Hou, Y. Zhou, W. Wang, and J. Yan, "Dense label encoding for boundary discontinuity free rotation detection," in *Proceedings of the IEEE/CVF conference on computer vision and pattern recognition*, 2021, pp. 15 819–15 829.
- [59] X. Yang, J. Yan, Q. Ming, W. Wang, X. Zhang, and Q. Tian, "Rethinking rotated object detection with gaussian wasserstein distance loss," in *International conference on machine learning*. PMLR, 2021, pp. 11 830–11 841.
- [60] X. Yang, X. Yang, J. Yang, Q. Ming, W. Wang, Q. Tian, and J. Yan, "Learning high-precision bounding box for rotated object detection via kullback-leibler divergence," *Advances in Neural Information Processing Systems*, vol. 34, pp. 18 381–18 394, 2021.
- [61] X. Yang, G. Zhang, X. Yang, Y. Zhou, W. Wang, J. Tang, T. He, and J. Yan, "Detecting rotated objects as gaussian distributions and its 3-d generalization," *IEEE Transactions on Pattern Analysis and Machine Intelligence*, vol. 45, no. 4, pp. 4335–4354, 2022.
- [62] J. Han, J. Ding, J. Li, and G. S. Xia, "Align deep features for oriented object detection," *IEEE Transactions on Geoscience and Remote Sensing*, pp. 1–11, 2021.
- [63] H. Zhang, "mixup: Beyond empirical risk minimization," *arXiv preprint arXiv:1710.09412*, 2017.
- [64] S. Yun, D. Han, S. J. Oh, S. Chun, J. Choe, and Y. Yoo, "Cutmix: Regularization strategy to train strong classifiers with localizable features," in *Proceedings of the IEEE/CVF international conference on computer vision*, 2019, pp. 6023–6032.
- [65] B. Zoph, E. D. Cubuk, G. Ghiasi, T.-Y. Lin, J. Shlens, and Q. V. Le, "Learning data augmentation strategies for object detection," in *Computer Vision—ECCV 2020: 16th European Conference, Glasgow, UK, August 23–28, 2020, Proceedings, Part XXVII 16*. Springer, 2020, pp. 566–583.
- [66] Y. Grandvalet and Y. Bengio, "Semi-supervised learning by entropy minimization," *Advances in neural information processing systems*, vol. 17, 2004.
- [67] D.-H. Lee *et al.*, "Pseudo-label: The simple and efficient semi-supervised learning method for deep neural networks," in *Workshop on challenges in representation learning, ICML*, vol. 3, no. 2. Atlanta, 2013, p. 896.
- [68] Q. Xie, M.-T. Luong, E. Hovy, and Q. V. Le, "Self-training with noisy student improves imagenet classification," in *Proceedings of the IEEE/CVF conference on computer vision and pattern recognition*, 2020, pp. 10 687–10 698.
- [69] D. Berthelot, N. Carlini, I. Goodfellow, N. Papernot, A. Oliver, and C. A. Raffel, "Mixmatch: A holistic approach to semi-supervised learning," *Advances in neural information processing systems*, vol. 32, 2019.
- [70] A. Tarvainen and H. Valpola, "Mean teachers are better role models: Weight-averaged consistency targets improve semi-supervised deep learning results," *Advances in neural information processing systems*, vol. 30, 2017.
- [71] Q. Xie, Z. Dai, E. Hovy, T. Luong, and Q. Le, "Unsupervised data augmentation for consistency training," *Advances in neural information processing systems*, vol. 33, pp. 6256–6268, 2020.
- [72] K. Sohn, D. Berthelot, N. Carlini, Z. Zhang, H. Zhang, C. A. Raffel, E. D. Cubuk, A. Kurakin, and C.-L. Li, "Fixmatch: Simplifying semi-supervised learning with consistency and confidence," *Advances in neural information processing systems*, vol. 33, pp. 596–608, 2020.
- [73] Y.-C. Liu, C.-Y. Ma, and Z. Kira, "Unbiased teacher v2: Semi-supervised object detection for anchor-free and anchor-based detectors," in *Proceedings of the IEEE/CVF Conference on Computer Vision and Pattern Recognition*, 2022, pp. 9819–9828.
- [74] Q. Yang, X. Wei, B. Wang, X.-S. Hua, and L. Zhang, "Interactive self-training with mean teachers for semi-supervised object detection," in *Proceedings of the IEEE/CVF conference on computer vision and pattern recognition*, 2021, pp. 5941–5950.
- [75] W. Hua, D. Liang, J. Li, X. Liu, Z. Zou, X. Ye, and X. Bai, "Sood: Towards semi-supervised oriented object detection," in *Proceedings of the IEEE/CVF Conference on Computer Vision and Pattern Recognition*, 2023, pp. 15 558–15 567.
- [76] C. Xi, Z. Wang, W. Wang, X. Xie, J. Kang, and R. Fernandez-Beltran, "Cromoda: Unsupervised oriented sar ship detection via cross-modality distribution alignment," *IEEE Journal of Selected Topics in Applied Earth Observations and Remote Sensing*, 2024.
- [77] K. Wang, Z. Xiao, Q. Wan, F. Xia, P. Chen, and D. Li, "Global focal learning for semi-supervised oriented object detection," *IEEE Transactions on Geoscience and Remote Sensing*, vol. 62, pp. 1–13, 2024.
- [78] Y. Wang, L. Yao, X. Zhang, J. Song, and H. Zhang, "Mining oriented information for semi-supervised object detection in remote sensing images," in *2024 International Joint Conference on Neural Networks (IJCNN)*, 2024, pp. 1–8.
- [79] R. Fu, S. Yan, C. Chen, X. Wang, A. A. Heidari, J. Li, and H. Chen, "S²o-det: A semisupervised oriented object detection network for remote sensing images," *IEEE Transactions on Industrial Informatics*, vol. 20, no. 9, pp. 11 285–11 294, 2024.
- [80] D. Liang, W. Hua, C. Shi, Z. Zou, X. Ye, and X. Bai, "Sood++: Leveraging unlabeled data to boost oriented object detection," *arXiv preprint arXiv:2407.01016*, 2024.
- [81] A. Zareian, K. D. Rosa, D. H. Hu, and S.-F. Chang, "Open-vocabulary object detection using captions," in *Proceedings of the IEEE/CVF Conference on Computer Vision and Pattern Recognition*, 2021, pp. 14 393–14 402.
- [82] A. Radford, J. W. Kim, C. Hallacy, A. Ramesh, G. Goh, S. Agarwal, G. Sastry, A. Askell, P. Mishkin, J. Clark *et al.*, "Learning transferable visual models from natural language supervision," in *International conference on machine learning*. PMLR, 2021, pp. 8748–8763.
- [83] Y. Du, F. Wei, Z. Zhang, M. Shi, Y. Gao, and G. Li, "Learning to prompt for open-vocabulary object detection with vision-language model," in *Proceedings of the IEEE/CVF Conference on Computer Vision and Pattern Recognition*, 2022, pp. 14 084–14 093.
- [84] C. Feng, Y. Zhong, Z. Jie, X. Chu, H. Ren, X. Wei, W. Xie, and L. Ma, "Promptdet: Towards open-vocabulary detection using uncurated images," in *European Conference on Computer Vision*. Springer, 2022, pp. 701–717.
- [85] Y. Zang, W. Li, K. Zhou, C. Huang, and C. C. Loy, "Open-vocabulary detr with conditional matching," in *European Conference on Computer Vision*. Springer, 2022, pp. 106–122.
- [86] X. Wu, F. Zhu, R. Zhao, and H. Li, "Cora: Adapting clip for open-vocabulary detection with region prompting and anchor pre-matching," in *Proceedings of the IEEE/CVF Conference on Computer Vision and Pattern Recognition*, 2023, pp. 7031–7040.
- [87] H. Zhang, P. Zhang, X. Hu, Y.-C. Chen, L. Li, X. Dai, L. Wang, L. Yuan, J.-N. Hwang, and J. Gao, "Glipv2: Unifying localization and vision-language understanding," *Advances in Neural Information Processing Systems*, vol. 35, pp. 36 067–36 080, 2022.
- [88] J. Pan, Y. Liu, Y. Fu, M. Ma, J. Li, D. P. Paudel, L. Van Gool, and X. Huang, "Locate anything on earth: Advancing open-vocabulary object detection for remote sensing community," *arXiv preprint arXiv:2408.09110*, 2024.
- [89] G. Wei, X. Yuan, Y. Liu, Z. Shang, K. Yao, C. Li, Q. Yan, C. Zhao, H. Zhang, and R. Xiao, "Ova-detr: Open vocabulary aerial object detection using image-text alignment and fusion," 2024. [Online]. Available: <https://arxiv.org/abs/2408.12246>
- [90] K. He, H. Fan, Y. Wu, S. Xie, and R. Girshick, "Momentum contrast for unsupervised visual representation learning," in *Proceedings of the IEEE/CVF conference on computer vision and pattern recognition*, 2020, pp. 9729–9738.
- [91] S. Zhao, Z. Zhang, S. Schuster, L. Zhao, B. Vijay Kumar, A. Stathopoulos, M. Chandraker, and D. N. Metaxas, "Exploiting unlabeled data with vision and language models for object detection," in *European Conference on Computer Vision*. Springer, 2022, pp. 159–175.
- [92] Y. Zhou, X. Yang, G. Zhang, J. Wang, Y. Liu, L. Hou, X. Jiang, X. Liu, J. Yan, C. Lyu, W. Zhang, and K. Chen, "Mmrotate: A rotated object detection benchmark using pytorch," in *Proceedings of the 30th ACM International Conference on Multimedia*, 2022.
- [93] G. Cheng, J. Han, and X. Lu, "Remote sensing image scene classification: Benchmark and state of the art," *Proceedings of the IEEE*, vol. 105, no. 10, pp. 1865–1883, 2017.
- [94] K. Chen, J. Wang, J. Pang, Y. Cao, Y. Xiong, X. Li, S. Sun, W. Feng, Z. Liu, J. Xu, Z. Zhang, D. Cheng, C. Zhu, T. Cheng, Q. Zhao, B. Li, X. Lu, R. Zhu, Y. Wu, J. Dai, J. Wang, J. Shi, W. Ouyang, C. C. Loy, and D. Lin, "MMDetection: Open mmlab detection toolbox and benchmark," *arXiv preprint arXiv:1906.07155*, 2019.
- [95] K. He, X. Zhang, S. Ren, and J. Sun, "Deep residual learning for image recognition," in *Proceedings of the IEEE conference on computer vision and pattern recognition*, 2016, pp. 770–778.
- [96] S. Rahman, S. Khan, and F. Porikli, "Zero-shot object detection: Learning to simultaneously recognize and localize novel concepts," in *Asian Conference on Computer Vision*. Springer, 2018, pp. 547–563.
- [97] Y. Zheng, R. Huang, C. Han, X. Huang, and L. Cui, "Background learnable cascade for zero-shot object detection," in *Proceedings of the Asian Conference on Computer Vision*, 2020.

- [98] S. Wu, W. Zhang, S. Jin, W. Liu, and C. C. Loy, "Aligning bag of regions for open-vocabulary object detection," in *CVPR*, 2023.
- [99] T. Cheng, L. Song, Y. Ge, W. Liu, X. Wang, and Y. Shan, "Yolo-world: Real-time open-vocabulary object detection," in *Proc. IEEE Conf. Computer Vision and Pattern Recognition (CVPR)*, 2024.
- [100] H. Bilen and A. Vedaldi, "Weakly supervised deep detection networks," in *Proceedings of the IEEE conference on computer vision and pattern recognition*, 2016, pp. 2846–2854.
- [101] K. Ye, M. Zhang, A. Kovashka, W. Li, D. Qin, and J. Berent, "Cap2det: Learning to amplify weak caption supervision for object detection," in *Proceedings of the IEEE/CVF International Conference on Computer Vision*, 2019, pp. 9686–9695.